INFRARED RADIATIVE ENERGY TRANSFER

IN GASES

by

R.D. CESS and S.N. TIWARI
College of Engineering
State University of New York, Stony Brook

Prepared for Publication in
ADVANCES IN HEAT TRANSFER, Volume VIII
Academic Press, New York

Supported by
The National Science Foundation
Grant Number GK-16755

May 1971

CONTENTS

I. INTRODUCTION

The object of this article is to illustrate the incorporation of spectroscopic information into the radiative transfer equations, and to present a reasonable means of treating radiative energy transfer within gases. Specific restriction is made to infrared gaseous radiation, which results from molecular transitions involving both vibrational and rotational energies, and emphasis will be placed upon the application of molecular band models to radiative transfer analyses. In a sense, the present chapter may be regarded as a continuation of the chapter appearing in Volume 5 of Advances in Heat Transfer by C.L. Tien, within which detailed information regarding vibration-rotation bands is included. Consequently, the present chapter will only briefly review vibration-rotation spectra, while the main objective will be to apply band information to the formulation of radiative energy transfer within gases, i.e., to the application of local conservation of energy within a gas.

The chapter is divided into several sections, and the following section, Section II, briefly reviews infrared band spectra, introduces very simple band models, and proceeds to discuss the formulation of total band absorptance information with the aid of these models. The basic equations describing radiative transfer within an infrared absorbing-emitting gas are formulated in Section III, and these allow for radiatively induced departures from local thermodynamic equilibrium. The final section, Section IV, presents some illustrative radiative transfer analyses, with emphasis upon physical interpretations and the relative importance of thermal radiation versus molecular conduction as energy transport mechanisms.

II. BAND ABSORPTANCE MODELS

The purpose of this section is to formulate and discuss spectroscopic models describing the total band absorptance for infrared radiating gases. As will be seen in Section III, the total band absorptance plays an essential role in describing the equations for the radiative energy flux. First, however, it will be necessary to review briefly several aspects of the basic structure of vibration-rotation bands. As previously discussed, no attempt at completness will be made, since a description of infrared band structure has been given in the article by Tien (1).

A. BAND ABSORPTION

Infrared absorption and emission of thermal radiation is a consequence of coupled vibrational and rotational energy transitions. Quite obviously, a diatomic molecule is the simplest molecule which will undergo such transitions. However, symmetric diatomic molecules, such as O_2 and N_2, have no permanent dipole moment, and thus they are transparent to infrared radiation.[1] For unsymmetric diatomic molecules, such as CO, the infrared spectrum will consist of a fundamental vibration-rotation band occurring at the fundamental vibrational frequency of the molecule; i.e., the band arises due to an energy transition between two adjacent vibrational energy levels. Vibrational transitions spanning three vibrational levels produce the first overtone band located at twice the fundamental frequency of the molecule, and subsequent overtone bands occur at higher multiples of the

[1] Symmetric diatomic molecules may have pressure-induced bands which can play a significant role in atmospheric radiation. For example, infrared transmission by hydrogen is important in the atmospheres of the Jovian planets (2,3).

fundamental frequency. In general, the overtone bands are quite insignificant relative to the fundamental band.

The picture is much the same for polyatomic molecules, except that these have more vibrational degrees of freedom. For example, carbon dioxide is a linear triatomic molecule and thus possesses four vibrational degrees of freedom. The two bending frequencies, however, are identical, while one of the stretching modes is symmetric and thus has no permanent dipole moment. Consequently, carbon dioxide has two fundamental bands. In addition to fundamental and overtone bands, the infrared spectrum of polyatomic molecules also includes combination and difference bands which occur at linear combinations or differences of the fundamental frequencies. Again choosing carbon dioxide as an example, the important infrared bands are the 15μ and 4.3μ fundamental bands and the 2.7μ combination band.

While the location of a vibration-rotation band is described by the associated vibrational transition, the band structure is governed by simultaneous rotational transitions which accompany a vibrational transition. As a consequence of the unequal spacing of rotational energy levels, the coupled vibration-rotation transitions occur at discrete frequencies located about the vibrational frequency. The resulting band structure in turn consists of an array of discrete rotational lines.

Before proceeding, it should be mentioned that while a vibrational transition is always coupled with a rotational transition, rotational transitions do occur by themselves. Since the transition energies are very small, the resulting spectrum is normally in the microwave region and has no influence on infrared radiation. There are exceptions, such as water vapor which possesses a pure rotation band in the far infrared.

Often, however, this pure rotation band is treated in a manner similar to a vibration-rotation band.

In order to describe the absorption characteristics of a vibration-rotation band, it is first necessary to consider the variation of the spectral absorption coefficient for a single line. For infrared radiation, the most important line-broadening mechanism is pressure broadening (1), and the variation of the spectral absorption coefficient with wave number is given by the Lorentz line profile as

$$\frac{\kappa_{\omega j}}{P} = \frac{S_j}{\pi} \frac{\gamma_j}{\gamma_j^2 + (\omega - \omega_j)^2} \tag{1}$$

Here κ_ω denotes the volumetric absorption coefficient, and ω is wave number ($\omega = \nu/c$ where c is the speed of light and ν the frequency). The rotational quantum number is denoted by j, such that the subscript j refers to a specific line within the band. Thus the wave number location of the line is ω_j, and γ_j and S_j refer to the half width and intensity of the line, respectively. For the time being, no distinction will be made between total and partial pressures. The line intensity is defined as

$$S_j = \int_{-\infty}^{\infty} \frac{\kappa_{\omega j}}{P} \, d\,(\omega - \omega_j) \tag{2}$$

and this is consistent with eq. (1). The line intensity may be described in terms of the molecular number density and Einstein coefficients, and for a perfect gas it follows that S_j is a function solely of temperature.

From kinetic theory, the line half width may be shown to vary with pressure and temperature as

$$\gamma_j \sim \frac{P}{\sqrt{T}} \tag{3}$$

More detailed quantum mechanical calculations again show the linear dependency upon pressure, but indicate that the inverse square-root variation with temperature is often true only for the band wings (large values of j). Again considering CO_2 as an example, Yamamoto, Tanaka, and Aoki (4) have shown that the temperature dependency of the line half width may be described by $\gamma_j \sim T^{-n_j}$, and that n_j approaches 0.75 for small j, decreases with increasing j to approximately 0.3, and then increases with a further inarease in j to the kinetic theory value of 0.5.

The Lorentz line profile, as described by eq. (1), is illustrated in Fig. 1. There are two points worth noting. The first is that increasing pressure broadens the line, and, with respect to a complete band consisting of many lines, this will at sufficiently high pressures lead to a smearing out of the discrete line structure. The second point is that the maximum absorption coefficient, which occurs at $\omega = \omega_j$, is invariant with pressure, since

$$(\kappa_{\omega j})_{\omega=\omega_j} = \frac{PS_j}{\pi\gamma_j} \tag{4}$$

from eq. (1), while $\gamma_j \sim P$.

It remains to describe the variation of line intensity with rotational quantum number, and for present purposes the simple model of a harmonic oscillator and rigid rotor will be assumed. Following Penner (5), and assuming a large number of lines (large j), the variation of S_j with j is

$$S_j = \frac{ShcBj}{kT} \exp\left(-\frac{hcBj^2}{kT}\right) \tag{5}$$

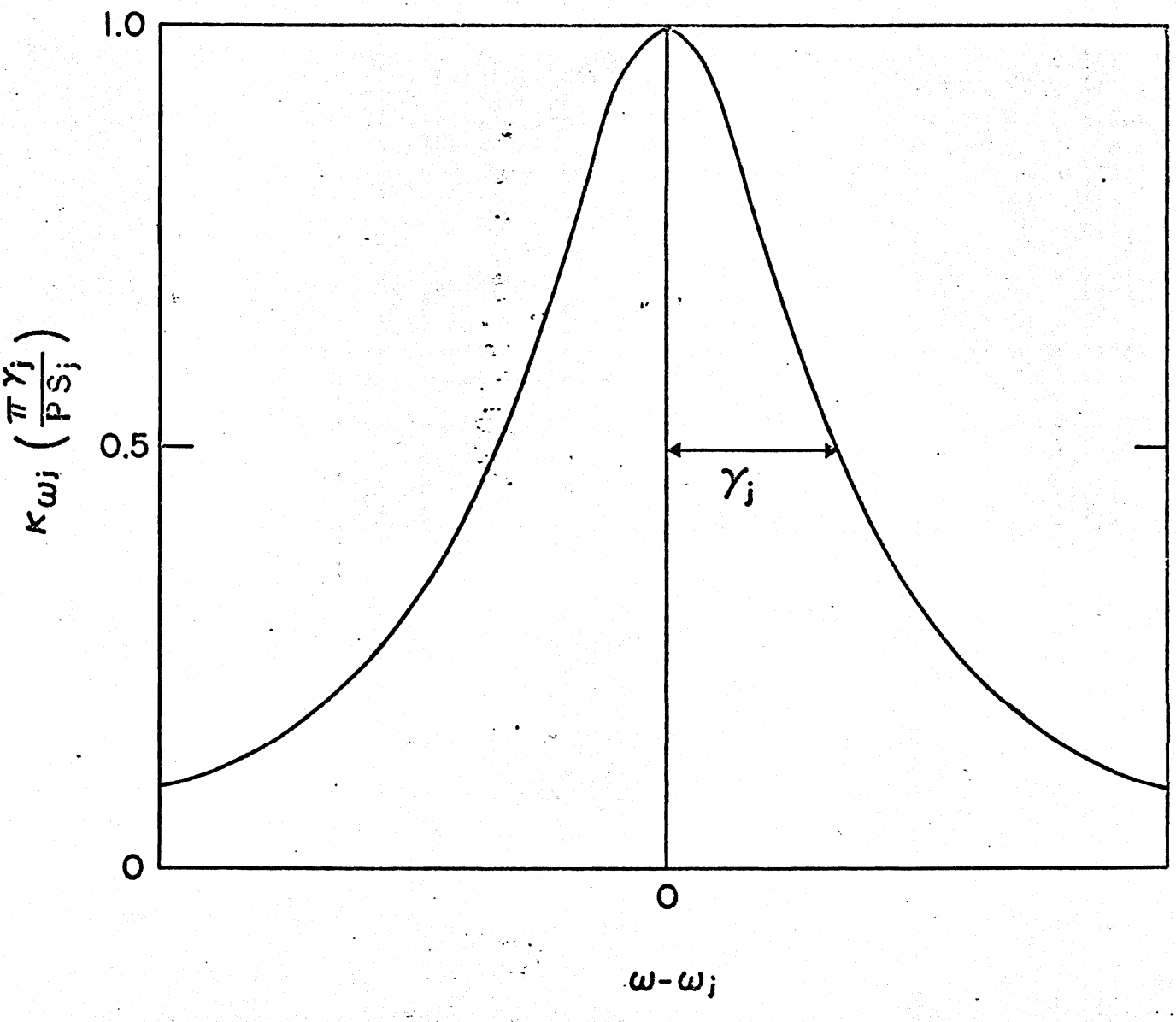

Fig. 1. Lorentz line profile.

where h is Planck's constant, k Boltzmann's constant, and B the rotational constant of the molecule. Furthermore, S denotes the intensity of the total band, such that

$$S = \int_{-\infty}^{\infty} \frac{\kappa_\omega}{P} \, d(\omega - \omega_o) \tag{6}$$

where ω_o is the wave number at the band center. It should be realized, of course, that the integration limits in eq. (6) imply integration over the entire band, as opposed to eq. (2), where the limits indicate integration over a single line.

A further consequence of the rigid-rotor approximation is that the lines are equally spaced, with the spacing d = 2B. Consequently, the line locations may be expressed in terms of wave number by

$$\omega - \omega_o = \pm 2jB \tag{7}$$

Combination of eqs. (6) and (7) allows a continuous representation of S_j with wave number, and this is illustrated in Fig. 2. In actuality, for a real band the two branches (P and R branches) are not symmetric, while vibrational modes involving bending exhibit a third central branch (Q branch). Nevertheless, the present simplified model will serve the purpose for which it is intended; i.e., to illustrate the basic features of the total band absorptance.

With regard to the variation of κ_ω over the entire band, this will consist of the superposition of the contributions from the individual lines, such that

$$\kappa_\omega = \sum_j \kappa_{\omega j} = \frac{P}{\pi} \sum_j \frac{S_j \gamma_j}{\gamma_j^2 + (\omega - \omega_j)^2} \tag{8}$$

It is further apparent that

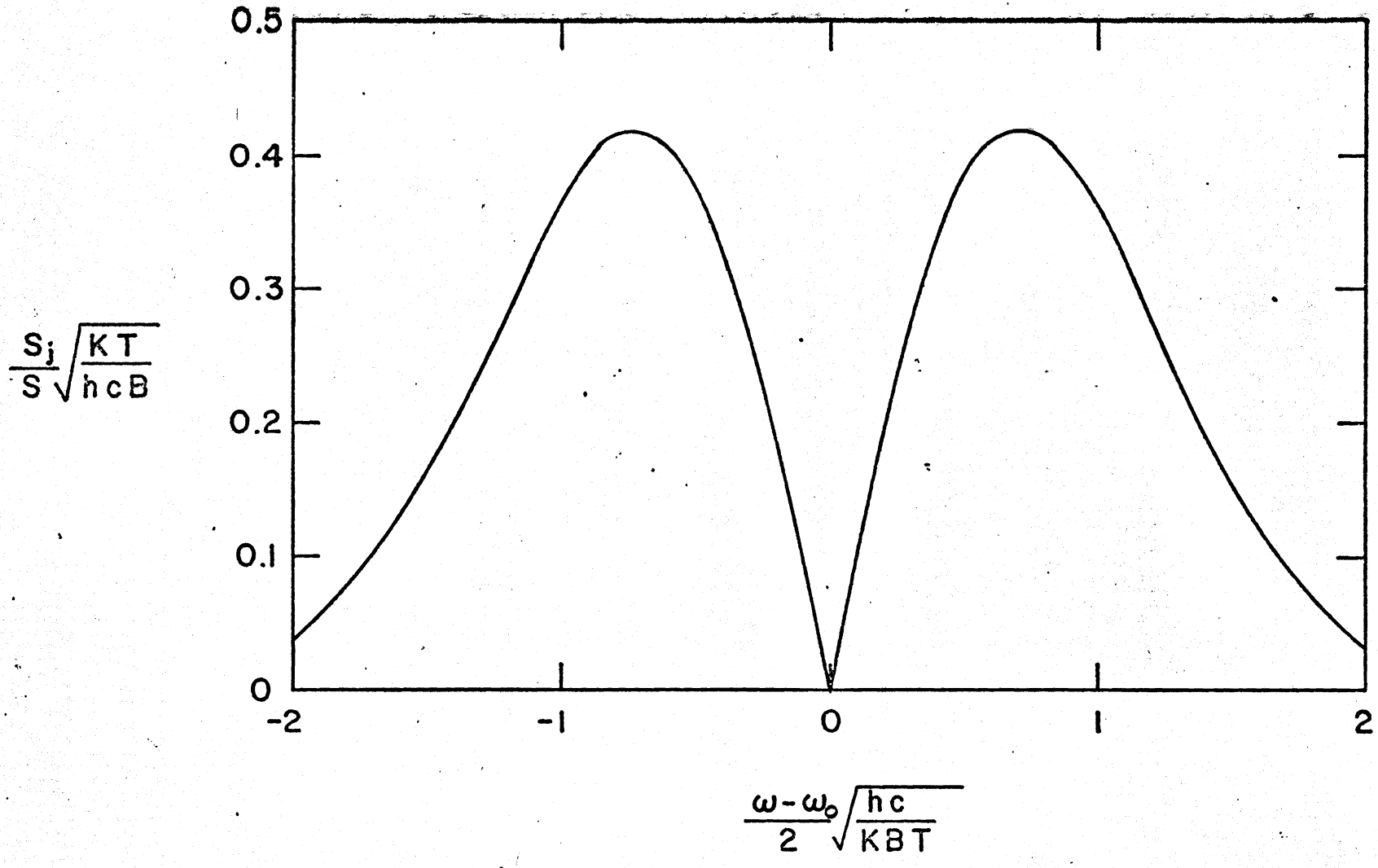

Fig. 2. Variation of S_j for a harmonic oscillator and rigid rotor.

$$S = 2 \sum_{j=o}^{\infty} S_j$$

where the factor of two is included to account for both branches. Again assuming a large number of lines, the summation may be replaced by integration, and employing eq. (5)

$$S = 2 \int_o^{\infty} S_j dj = S$$

which illustrates that the separate applications of the assumption of a large number of lines are mutually compatible. Since S_j is a function solely of temperature, the above equation additionally illustrates that the band intensity is a function only of temperature.[2]

B. BAND ABSORPTANCE

The spectral band absorptance is defined as

$$\alpha_\omega = 1-e^{-\kappa_\omega y} \tag{9}$$

The physical interpretation of α_ω is that it is the fraction of energy which is absorbed when a beam of radiant energy passes through an isothermal slab of gas of thickness y. The total band absorptance is in turn

$$A = \int_{-\infty}^{\infty} \alpha_\omega \, d(\omega-\omega_o) \tag{10}$$

where the integration over the single band is again implied. The physical interpretation of the total band absorptance is not as simple as for its spectral counterpart a_ω. For present purposes, it will be sufficient to

---

[2] While the conclusion is correct, the situation is really not this simple, since summation over vibrational quantum number has been ignored.

state that the total band absorptance will be needed later to generate the kernel function in the radiative flux equations.

A convenient form of eq. (10) follows to be

$$A = \int_{-\infty}^{\infty} [1-\exp(-\frac{K_W}{P} Py)] \, d(\omega-\omega_o) \tag{11}$$

From eq. (8) it is evident that K_W/P depends both upon pressure and temperature, such that

$$A = A(Py, P, T) \tag{12}$$

It is important to note the dual role that pressure plays. Its appearance in the pressure path length, Py, is due simply to the fact that absorption is dependent upon the number of molecules which are present along a line of sight. The second dependency upon pressure is a result of the line structure of the band being a function of pressure. For sufficiently high pressures the line structure is smeared out, and in this limit pressure enters solely through the pressure path length Py. This will be illustrated in quantitative terms later.

In the following two subsections, simple band models will be employed to illustrate certain basic features of the total band absorptance. There is, however, one important limiting form of A which is completely independent of the band model, and this applies when $K_\omega y << 1$; i.e., for the conventional optically thin limit in radiative transfer. Upon expanding the exponential in eq. (11), then

$$A = Py \int_{-\infty}^{\infty} \frac{K_\omega}{P} \, d(\omega-\omega_o) = PyS \tag{13}$$

This is the so-called linear limit, and the important feature of this limit is the fact that the total band absorptance is independent of

rotational line structure.

A second limiting form for the total band absorptance is that of strong nonoverlapping lines. Although the actual limiting result for A depends upon the band model employed, the conditions for achieving this limit may be discussed in general terms. The limit requires that two separate conditions be satisfied. The first is the requirement of strong lines, for which total absorption occurs in the vicinity of the line centers. From eq. (9), this is equivalent to requiring that $\kappa_{\omega j} y >> 1$ for $\omega=\omega_j$, and upon combining this with eq. (4), the strong line condition becomes

$$\frac{S_j P y}{\pi \gamma_j} >> 1 \tag{14}$$

The second condition pertains to nonoverlapping lines, and the motivation for this limit is to be able to employ the expression

$$A = \sum_j A_j \tag{15}$$

where A_j is the total absorptance of a single line

$$A_j = \int_{-\infty}^{\infty} (1-e^{-\kappa_{\omega j} y}) \, d(\omega-\omega_j) \tag{16}$$

with the integration being performed over the individual lines. Equation (15) is, of course, applicable only if the integrands in eq. (16) do not overlap, since eq. (15) constitutes simply a summation of individual line absorptances. What is required, then, is that the integrand in eq. (16) approach zero for $w-w_j = O(d)$, where d is the line spacing. With reference to eq. (1), the nonoverlapping line limit will be satisfied providing

$$\frac{S_j P y}{\pi} \frac{\gamma_j}{\gamma_j^2+d^2} << 1 \tag{17}$$

At this point, it should be noted that if we were to allow $\gamma_j \geq O(d)$, then eq. (17) would yield

$$\frac{S_j P y}{\pi \gamma_j} << 1$$

and this is a direct contradiction to the strong line condition of eq. (14). Hence, to avoid this contradiction it is necessary to require that $\gamma_j << d$. The conditions which must be satisfied in order to achieve nonoverlapping lines are thus

$$\frac{\gamma_j}{d} << 1 , \quad \frac{S_j P y \gamma_j}{\pi d^2} << 1 \tag{18}$$

where the second condition follows from eq. (17). The above conditions, together with eq. (14), describe the strong nonoverlapping line limit. The application of these three conditions in deriving this limit will be illustrated in the following subsection.

C. ELSASSER MODEL

The simplest band model that accounts for line structure is the Elsasser model, for which equally spaced lines of equal intensity and equal half width are assumed. A portion of such a band is illustrated in Fig. 3, where the broken curves represent the absorption coefficient of the individual lines, while the solid curve is the absorption coefficient as given by eq. (8), and this may be rephrased as

$$\frac{\kappa_\omega}{P} = \frac{S_j \gamma}{\pi} \sum_{j=o}^{\infty} \frac{1}{\gamma^2 + (\omega - \omega_o \pm jd)^2} \tag{19}$$

The subscript j has been dropped from y_j in accord with the previous

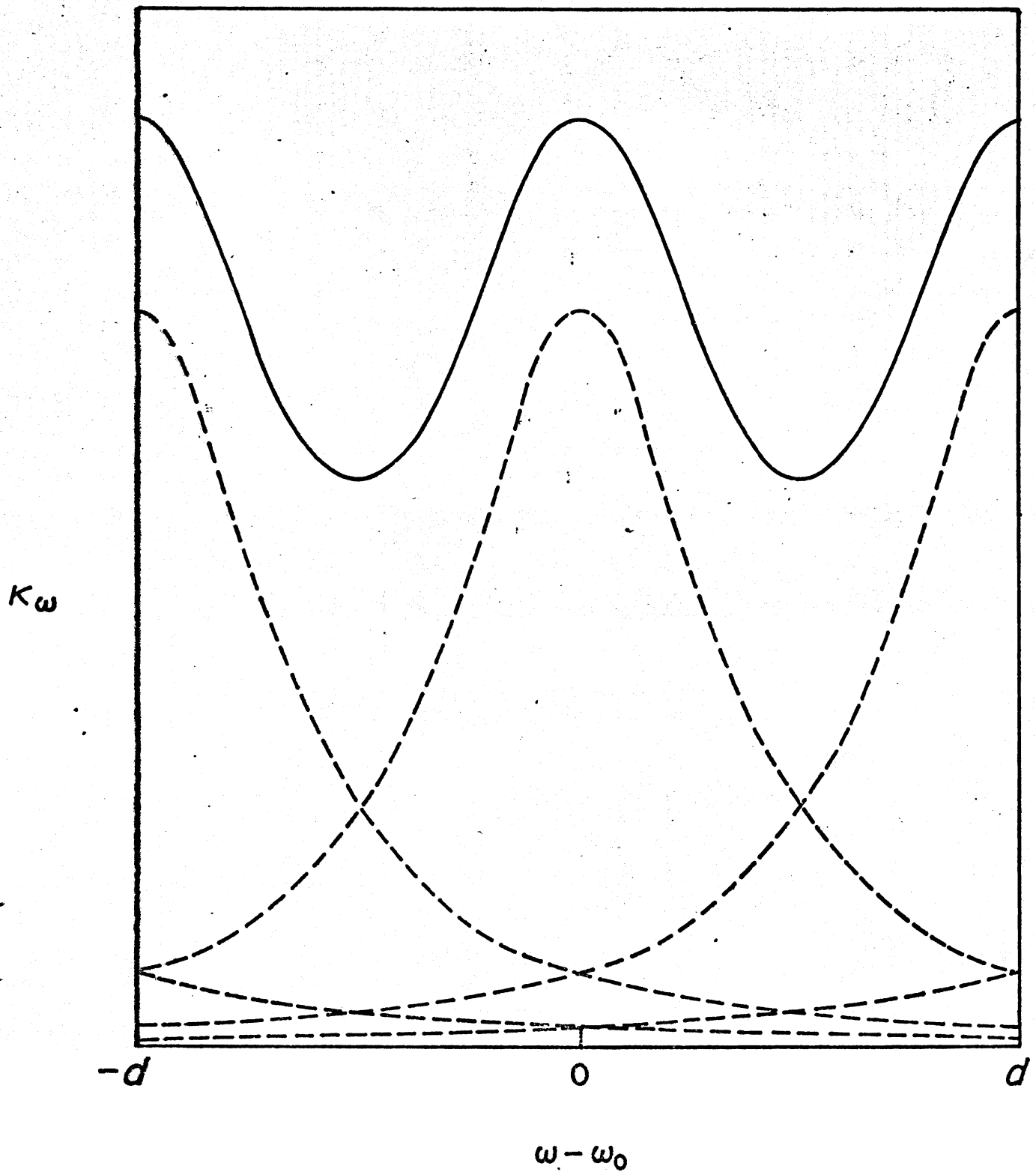

Fig. 3. Elsasser band model..

assumption, but it is retained in S_j, even though S_j is independent of j, in order to denote that this is a line intensity. Carrying the summation to infinity does not preclude restriction to a finite band width (finite number of lines), but is merely consistent with the earlier assumption of a large number of lines. The above series may be expressed in closed form as (6)

$$\frac{\kappa_\omega}{P} = \frac{S_j}{d}\left[\frac{\sinh(\pi\beta/2)}{\cosh(\pi\beta/2)-\cos(\pi z/2)}\right] \tag{20}$$

where

$$\beta = \frac{4\gamma}{d}, \quad z = \frac{4(\omega-\omega_o)}{d}.$$

The quantity β is a particularly significant parameter, since it represents the role of line structure. Recalling that $\gamma \sim P$, the limit of large pressure corresponds to $\beta \to \infty$. This is the limit for which line structure is smeared out, and eq. (20) reduces to

$$\frac{\kappa_\omega}{P} = \frac{S_j}{d} \tag{21}$$

The ratio S_j/d also has an alternate interpretation. If an average absorption coefficient is defined over a line spacing as

$$\frac{\overline{\kappa}_\omega}{P} = \frac{1}{d}\int_{-d/2}^{d/2} \frac{\kappa_\omega}{P}\, d\,(\omega-\omega_j)$$

it follows from eq. (20) that $\overline{\kappa}_\omega/P = S_j/d$.

The wave number width of the total band will be denoted by A_o, and letting n be the number of lines in the band, then $A_o = nd$. Furthermore

$$S = \sum_j S_j = nS_j$$

and the total absorptance of the Elsasser band follows from eqs. (11) and (20) to be

$$A = \frac{A_o}{2} \int_o^2 \{1-\exp[-\frac{u \sinh(\pi\beta/2)}{\cosh(\pi\beta/2)-\cos(\pi z/2)}]\}dz \qquad (22)$$

where u is a dimensionless pressure path length defined by

$$u = \frac{SPy}{A_o}$$

Equation (22) has a form that is characteristic of all band models, namely that the total absorptance may be expressed as

$$A = A_o \bar{A}(u,\beta) \qquad (23)$$

where $\bar{A}(u,\beta)$ is a dimensionless function. Recall from the previous discussion that pressure enters into the band absorptance in two ways, both through the pressure path length and a line structure effect. This dual role is clearly illustrated by eq. (23), since u is a dimensionless pressure path length, while β is a line structure parameter.

Consider now limiting forms of the total band absorptance. The linear limit, applicable for $u << 1$, readily follows from eq. (22) to be

$$\bar{A} = u \; ; \quad u << 1 \qquad (24)$$

and this is consistent with eq. (13). Note once again that line structure plays no role in the limit of small path lengths. In the large path length limit, $u >> 1$, and eq. (22) yields

$$\bar{A} = 1 \; ; \quad u >> 1 \qquad (25)$$

Physically, of course, this represents total absorption within the finite-width band. It should be emphasized, however, that more realistic band

models yield considerably different results, as will be illustrated in the next subsection.

A third limit corresponds to strong nonoverlapping lines, and following Penner (5) or Goody (6), eq. (22) may be reduced to

$$\bar{A} = \text{erf}\left(\frac{1}{2}\sqrt{\frac{\pi u \beta}{2}}\right) \tag{26}$$

subject to certain constraints. As discussed by Penner (5), these consist of $\beta << 1$ and $u/\beta >> 1$. With reference to eqs. (14) and (18), the remaining requirement for the strong nonoverlapping line limit is $\beta u << 1$, for which eq. (26) yields

$$\bar{A} = \sqrt{\beta u}; \quad \beta << 1, \; u/\beta >> 1, \; \beta u << 1 \tag{27}$$

This is also referred to as the square-root limit.

A final limiting form of eq. (22) is that for which line structure is smeared out, and letting $\beta \to \infty$, then

$$\bar{A} = 1 - e^{-u} \; ; \; \beta >> 1 \tag{28}$$

As should be expected, this is simply Beer's law.

The Elsasser band absorptance is illustrated in Fig. 4, and the various limiting forms are clearly evident. For $u << 1$, the linear limit, $\bar{A} = u$, is obtained, with the band absorptance being independent of line structure. The three constraints on the square-root limit are also apparent. This limit requires $\beta << 1$, but it still departs from the complete solution for either large or small u. The departure for small u denotes a violation of the requirement that $u/\beta >> 1$, such that the strong line condition is no longer satisfied. For large u, the condition $\beta u << 1$ is not fulfilled, and eq. (15) is no longer applicable. The present large

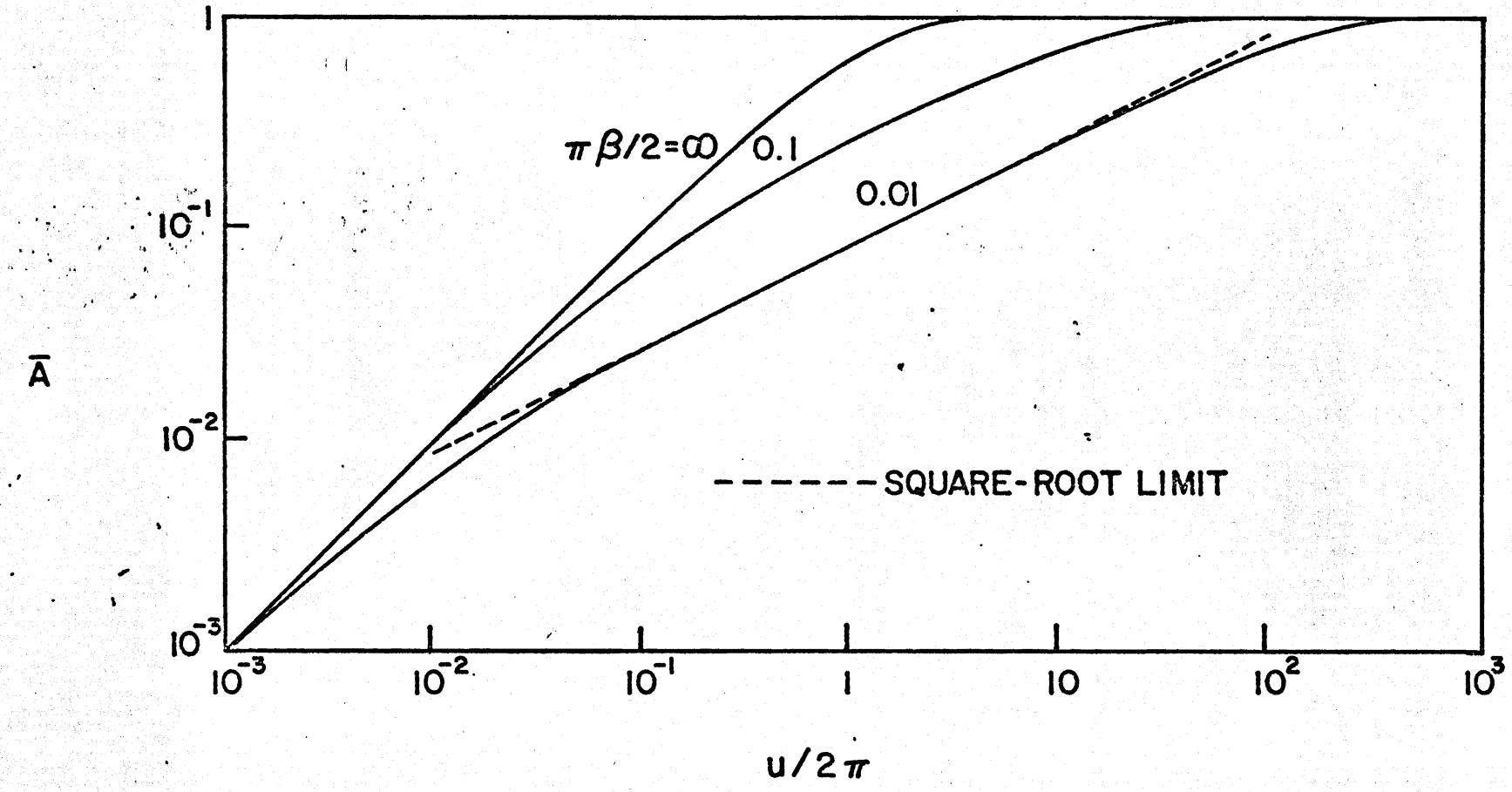

Fig. 4. Total band absorptance for Elsasser model.

path length limit, $\bar{A} = 1$, simply denotes total absorption within the band, and this is a consequence of the Elsasser model having a prescribed finite width. For a more realistic band model, as described in the following subsection, the total band absorptance will asymptotically approach a function of u rather than unity.

D. RIGID-ROTOR, HARMONIC-OSCILLATOR MODEL

Assuming the molecular model of a rigid rotor and harmonic oscillator, the distribution of line intensities is given by eq. (5), while the line spacing corresponds to eq. (7). Lorentz line shapes will again be assumed. In contrast to the Elsasser model, there is no defined band width, since the line intensities approach zero asymptotically in the band wings. Thus, the bandwidth parameter A_o will not correspond to a simple specified width, but instead will arise as an effective width resulting from the line intensity distribution of eq. (5). No attempt at a complete formulation of the total band absorptance will be made, however the limiting expressions will be presented. Since the linear limit is completely general, then eq. (24) is applicable to the present band model.

Considering the large path length limit ($u >> 1$), it will be convenient to initially assume a high pressure such that line structure is smeared out, which corresponds to the limit $\beta \to \infty$. Thus, in accord with eq. (21), and upon combining eqs. (5), (7), and (9), the spectral band absorptance is described by

$$a_\omega = 1 - \exp(-u\xi e^{-\xi^2}) \tag{29}$$

where again $u = SPy/A_o$, while

$$\xi = (\omega-\omega_o)/A_o$$

$$A_o = \sqrt{4kBT/hc} \tag{30}$$

Furthermore, since the band is symmetric, and with $\overline{A} = A/A_o$, then

$$\overline{A} = 2\int_o^\infty \alpha_\omega(\xi)d\xi \tag{31}$$

Combination of eqs. (29) and (31) thus describes the total band absorptance in the limit as $\beta \to \infty$, and numerical results are given by Penner (5). Concerning an asymptotic expression for large u, one procedure is to combine eqs. (29) and (31) and perform an asymptotic expansion. A physically more useful method, however, with reference to the inclusion of line structure, follows that employed by Edwards and Menard (7). Upon defining

$$\xi_1 = \sqrt{1nu}$$

eq. (31) may be written as

$$\overline{A} = 2\Gamma_1 + 2\Gamma_2 \tag{32}$$

where

$$\Gamma_1 = \int_o^{\xi_1} [1-\exp(-u\xi e^{-\xi^2})]d\xi$$

$$\Gamma_2 = \int_{51}^\infty [1-\exp(-u\xi e^{-\xi^2})]d\xi$$

It may readily be shown that for $u >> 1$

$$\Gamma_1 \to \sqrt{1nu} \tag{33a}$$

$$\Gamma_2 < 1/2 \tag{33b}$$

Thus, the large path length limit follows to be

$$\overline{A} = 2\sqrt{\ln u} \quad ; \quad u >> 1 \tag{34}$$

While eq. (34) has been derived subject to the condition $\beta \to \infty$, it is easily shown that this restriction may be removed. With reference to Fig. 5, Γ_1 denotes the area of the saturated portion of the band, and the inclusion of line structure will not alter eq. (33a) as a proper asymptotic limit. Thus, only Γ_2 will be affected. Again with reference to Fig. 5, if the region $5 > \xi_1$ is considered to consist of a series of Elsasser bands, it follows that the inclusion of line structure will result in a decrease in Γ_2, and eq. (33b) is again valid. Equation (34) therefore constitutes the asymptotic limit for the total band absorptance regardless of the value the line structure parameter β.

The third limit is the square-root limit, and recall that this corresponds to strong nonoverlapping lines. For strong lines, the Lorentz line profile, eq. (1), may be expressed by (6)

$$\frac{\kappa_{\omega j}}{P} = \frac{S_j \gamma_j}{(\omega - \omega_j)^2}$$

and upon substituting this into eq. (16)

$$A_j = 2\sqrt{S_j \gamma_j P y}$$

In turn, from eq. (15)

$$A = 2 \sum_{j=o}^{\infty} A_j = 4 \sum_{j=o}^{\infty} \sqrt{S_j \gamma_j P y} = 4 \sqrt{\gamma P y} \sum_{j=o}^{\infty} \sqrt{S_j}$$

where γ is a rotationally averaged mean line width defined by

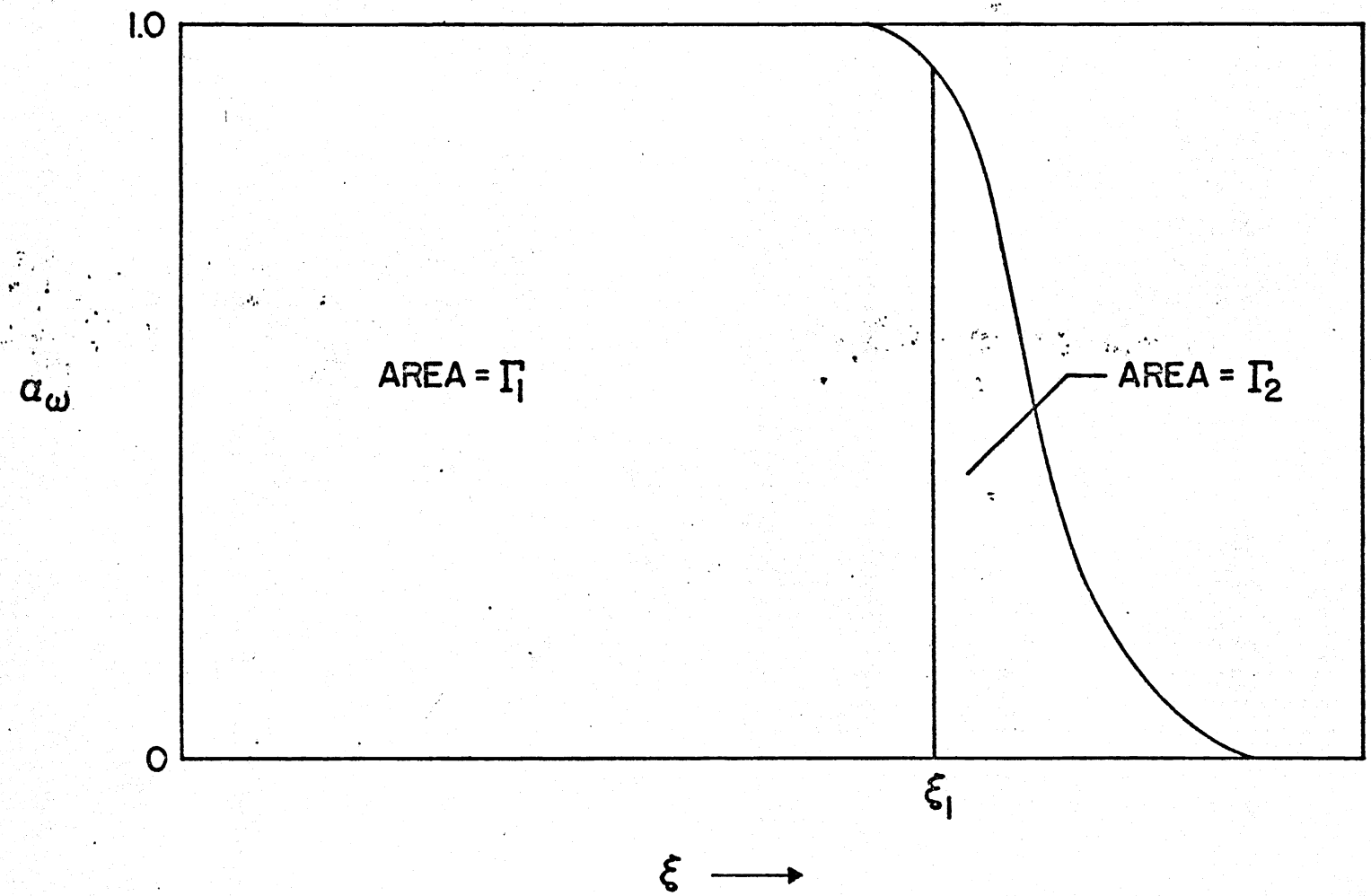

Fig. 5. Spectral band absorptance for large path lengths.

$$\sqrt{\gamma} = \frac{\sum_{j=o}^{\infty} \sqrt{\gamma_j S_j}}{\sum_{j=o}^{\infty} \sqrt{S_j}} \tag{35}$$

Again employing the assumption of a large number of lines, then

$$A = 4\sqrt{\gamma P y} \int_o^{\infty} \sqrt{S_j}\, dj$$

and upon combining this with (5), and noting from eq. (7) that d = 2B, it follows that

$$A = 2^{3/4}\, \Gamma(3/4) \sqrt{S P y A_o (4\gamma/d)} \tag{36}$$

At this point it should again be emphasized that summation over vibrational quantum number has not been taken into-account. While this has no direct bearing on the linear and large path length limits, since the band intensity S already denotes a summation over vibrational quantum number, it does affect the interpretation of the mean line width, Equation (36) is true only when all transitions have the same lower vibrational state, Upon letting v be the quantum number of the lower vibrational state, then eq. (36) should be recast as

$$A_v = 2^{3/4} \Gamma(3/4) \sqrt{S_v P y A_o (4\gamma/d)} \tag{37}$$

where S_v represents the distribution of intensity with vibrational quantum number, such that $S = \sum_{v=o}^{\infty} S_v$. It has been assumed in eq. (37) that the rotationally averaged line width y is independent of vibrational quantum number v, and this has been confirmed by Yamamato, Tanaka, and Aoki (4) for CO_2.

Following Edwards and Menard (8), and Edwards (9), it will further be assumed that rotational lines resulting from different vibrational

levels do not overlap, and the total band absorptance may thus be written as

$$A = \sum_{v=0}^{\infty} A_v \qquad (38)$$

From eq. (37), it follows that a vibrationally averaged mean line width may be defined as (8, 9)

$$\bar{\gamma} = \gamma\left(\sum_{v=0}^{\infty} \sqrt{S_v/S}\right)^2 \qquad (39)$$

Thus, upon letting $\beta = 4\bar{\gamma}/d$, the square-root limit follows from eqs. (37) and (38) to be

$$A = 2.06\sqrt{\beta u} \; ; \quad \beta << 1, \; u/\beta >> 1, \; \beta u << 1 \qquad (40)$$

At sufficiently low temperatures, for which only the vibrational ground state is populated, eq. (39) will reduce to $\bar{\gamma} = \gamma$. As temperature increases, however, the summation in eq. (39) will become a significant function of temperature, and the temperature dependence of $\bar{\gamma}$ may differ substantially from that of γ. To give an illustration, consider the 4.3μ fundamental band of CO_2. Employing the $\gamma_J(T)$ results of Yamamoto, Tanaka, and Aoki (4) in eq. (35), the temperature variation of $\gamma(T)$ may be expressed by

$$\gamma(T) = \gamma(T_o)\left(\frac{T}{T_o}\right)^{-2/3} \qquad (41)$$

and for temperatures of roughly 300°K and lower, this should adequately describe $\bar{\gamma}(T)$. Edwards and Menard (8), on the other hand, have found an average temperature dependence for the range 300°K to 1390°K of

$$\bar{\gamma} = \bar{\gamma}(T_o)\left(\frac{T}{T_o}\right)^{1/2} \qquad (42)$$

The discrepancy between eqs. (41) and (42) implies a rapid change in the temperature dependence of $\overline{\gamma}$ as temperature is increased.

The primary utility of the present molecular model of a rigid rotor and harmonic oscillator has been to illustrate limiting solutions of the total band absorptance for a semi-realistic molecular model. One important conclusion is that line structure appears only in the square-root limit, and thus this limit has been employed to describe the mean line width as defined by eqs. (35) and (39).

E. BAND ABSORPTANCE CORRELATIONS

While the preceding subsection dealt with limiting forms of the total band absorptance, it is necessary to have at hand an expression for $\overline{A}(u,\beta)$ which is applicable for all values of u and β. Several such expressions are available, and they are all based upon constructing an expression for $\overline{A}(u,\beta)$ which satisfies certain limiting conditions. For present purposes, the same limits as employed by Edwards and Menard (7) will be used, and these are

$$\overline{A} = u \quad ; \quad u \ll 1 \tag{43a}$$

$$\overline{A} = 2\sqrt{\beta u} \quad ; \quad \beta \ll 1, \quad u/\beta \gg 1, \quad \beta u \ll 1 \tag{43b}$$

$$\overline{A} = \ln u \quad ; \quad u \gg 1 \tag{43c}$$

While Edwards and Menard interpreted the above in terms of a reordered exponential distribution of line intensities, a slightly different explanation will be given here. The first limit, eq. (43a), is simply the general linear limit, while eq. (43b) is essentially eq. (40) for the rigid rotor and harmonic oscillator. The third limit is of a different

form than that of eq. (34) for the rigid rotor and harmonic oscillator. For moderately large values of u the two expressions are in reasonable numerical agreement, but for increasingly large u they begin to diverge. The rational for using eq. (43c) is twofold. First, Edwards and Menard have shown that a logarithmic limit is attained for nonrigid rather than rigid rotation, and second, existing emperical correlations are of the same form as eq. (43c).

The first band absorptance correlation to satisfy all three limits is that proposed by Edwards and Menard (7), and this consists of an analytic interpolation of the form

$\beta \leq 1$:

$$\bar{A} = u \quad ; \quad \bar{A} < \beta$$

$$\bar{A} = 2\sqrt{u\beta} - \beta \quad ; \quad \beta < \bar{A} < (2-\beta)$$

$$\bar{A} = \ln(\beta u) + (2-\beta) \quad ; \quad \bar{A} > (2-\beta)$$

$\beta > 1$:

$$\bar{A} = u \quad ; \quad \bar{A} < 1$$

$$\bar{A} = \ln u + 1 \quad ; \quad \bar{A} > 1$$

By comparing the above correlation with experimental data over a large range of pressure and temperature, Edwards and coworkers have empirically determined the necessary correlation quantities $S(T)$, $A_o(T)$, and $\beta(T,P_e)$, where P_e is the effective broadening pressure, for the important bands of CO, CO_2, H_2O, and CH_4. In determining $\beta(T,P_e)$, both self broadening and nitrogen broadening were considered. These results are summarized by Edwards, et al (10)[3]. In particular, for the CO fundamental and the 6.3μ

---

[3]The correlation quantities C_1 and C_3 of reference (10) correspond to the present nomenclature through $A_o = C_3$ and $S = C_1/RT$, where R is the gas constant.

fundamental of H_2O, it was found that

$$A_o = 1.91(kBT/hc)^{1/2} \tag{44}$$

and this is in excellent agreement with eq. (30).

A continuous band absorptance correlation has been proposed by Tien and Lowder (11), and this is of the form

$$\overline{A} = \ln\{uf(\beta)[\frac{u+2}{u+2f(\beta)}] + 1\} \tag{45}$$

where

$$f(\beta) = 2.94[1-\exp(-2.60\beta)]$$

The choice of eq. (45) was based on the specification of five conditions, and the form of $f(\beta)$ was chosen so as to give agreement with the correlation of Edwards and Menard. The square-root limit, eq. (43b), was not, however, one of the specified conditions, and eq. (45) does not satisfy this requirement.

A continuous correlation for $\overline{A}(u,\beta)$ has also been proposed by Goody and Belton (12), and in terms of the present nomenclature this may be written as

$$\overline{A} = 2 \ln [1 + \frac{\sqrt{\beta}\, u}{\sqrt{u+4\beta}}] \tag{46}$$

Although this correlation satisfies the three limits as specified by eqs. (43), there appears to be one shortcoming. Upon letting $\beta \to \infty$, which corresponds to smeared out line structure, eq. (46) reduces to

$$\overline{A} = 2 \ln (1+u)$$

and for large u this yields $2 \ln u$, while in the linear limit $2u$ is obtained. The linear and logarithmic limits are, however, independent of line structure,

such that eqs. (43a) and (43c) should be achieved irrespective of whether one does or does not let $\beta \to \infty$. Thus, it would appear that the use of eq. (46) should be restricted to relatively small values of β.

A fairly simple correlation, which does satisfy the above constraint, in addition to all of eqs. (43), is of the form

$$\overline{A} = 2 \ln\left[1 + \frac{u}{2 + \sqrt{u(1+1/\beta)}}\right] \tag{47}$$

Preliminary comparisons indicate that eq. (47) does an excellent job of correlating band absorptance data for CO_2.

III. BASIC EQUATIONS

In this section the basic equations will be developed which describe the radiative flux vector within an infrared absorbing-emitting gas. Knowledge of the radiative flux vector, $\underset{\sim}{q}_R$, is of course necessary in any conservation of energy analysis, since the energy equation for a radiatively participating gas is of the form

$$\frac{DT}{Dt} = \text{div}(\lambda \text{ grad } T) + \frac{DP}{Dt} - \text{div } \underset{\sim}{q}_R \qquad (48)$$

where ρ, c_p, and λ denote density, specific heat at constant pressure, and thermal conductivity, respectively. With reference to eq. (48), it is necessary to have a description of $\underset{\sim}{q}_R$ in terms of temperature within the gas, and this is precisely the purpose of the present section.

Strictly speaking, eq. (48) applies only to a molecular continuum under the condition of local thermodynamic equilibrium (LTE). The energy equation may, however, be extended to radiatively induced departures from LTE, and such extension is particularly appropriate to infrared transfer. This simply requires replacing $\underset{\sim}{q}_R$ in eq. (48) by its non-LTE counterpart. At the same time, however, it must be assumed that any departure from equilibrium population distributions will not significantly change the internal energy and transport properties from their equilibrium values. As discussed by Zel'dovich and Raizer (13), this assumption is justified providing the characteristic vibrational temperature $h\nu/k$ (where ν is a band frequency) is greater than the vibrational temperature. Thus, the temperature appearing in eq. (48) will be regarded as the kinetic temperature.

Radiatively induced departures from LTE occur when the gas molecules either emit or absorb radiative energy at such a high rate that collisional

equilibration cannot maintain a state of equilibrium between translational, vibrational, and rotational energies. Rotational energies, however, require only a few collisions to attain equilibrium, and significant departures from LTE will first involve solely vibrational energies. It may further be assumed that even for non-LTE, vibrational energy levels are populated according to the Boltzmann distribution. However, this distribution does not correspond to the local kinetic temperature, but instead is governed by a separate vibrational temperature.

In summary, the purpose of the present section is to develop an expression for the infrared radiative flux vector, and to allow in this development radiatively induced departures from vibrational equilibrium. In describing the radiative flux, the Kernel function will be expressed in terms of the total band absorptance. This approach is analogous to the LTE formulations of Goody (6), Gille and Goody (14), and Wang (15, 16), for which the Kernel function is expressed in terms of a modified gas emissivity. For present purposes, the physical model and coordinate system is that illustrated in Fig. 6. This consists of a gas bounded by two plates whose surfaces are assumed to be gray and to emit and reflect in a diffuse manner.

A. RATE EQUATIONS AND RELAXATION TIME

In considering radiatively induced vibrational nonequilibrium (non-LTE), it will be necessary to have information pertaining to vibrational rate equations and the vibrational relaxation time. The rate of change of vibrational energy of a system of oscillators may be expressed as

$$\frac{dE_v}{dt} = \left(\frac{dE_v}{dt}\right)_{coll} + \left(\frac{dE_v}{dt}\right)_{rad} \tag{49}$$

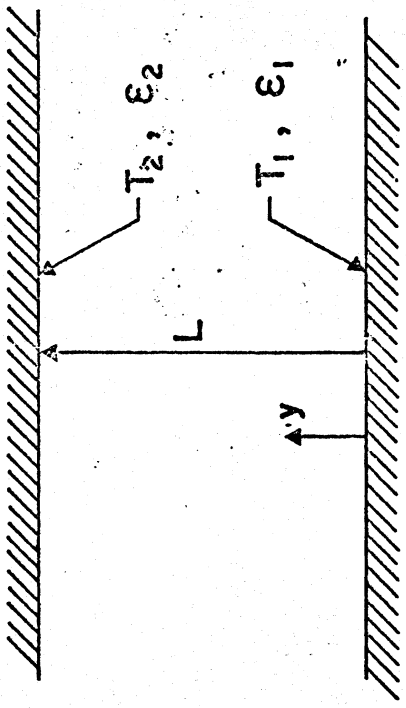

Fig. 6. Physical model and coordinate system.

where the terms on the right represent contributions due to collisional and radiative processes, respectively, and E_v denotes the vibrational energy per unit volume. Furthermore,

$$- \text{div } \underset{\sim}{q}_R = \left(\frac{dE_v}{dt}\right)_{rad} \tag{50}$$

where, due to the small separation of rotational levels, the contribution of rotational energy has been neglected.

The divergence of the radiative flux is also related to the specific intensity I_ω, and for the present one-dimensional problem this is given by the expression

$$\text{div } \underset{\sim}{q}_R = \int_o^\infty \frac{dq_{R\omega}}{dy}\, do = \int_o^\infty \int_o^{4\pi} \frac{dI_\omega}{ds}\, d\Omega d\omega \tag{51}$$

where Ω is the solid angle and s a coordinate measured along the pencil of rays. Combination of eqs. (49) through (51) thus yields

$$\frac{dE_v}{dt} = \left(\frac{dE_v}{dt}\right)_{coll} - \int_o^\infty \int_o^{4\pi} \frac{dI_\omega}{ds}\, d\Omega d\omega \tag{52}$$

This relation clearly illustrates the influence of radiation, through the second term on the right side, upon vibrational energy.

The vibrational relaxation of a system of oscillators undergoing collisional relaxation may be described in terms of the Bethe-Teller relation

$$\frac{dE_v}{dt} = \frac{E_v^* - E_v}{\eta} \tag{53}$$

where E_v^* represents the equilibrium value of vibrational energy, and η is the vibrational relaxation time. A simple derivation of eq. (53) is given by Zel'dovich and Raizer (13), and by Vincenti and Kruger (17),

while anharmonic effects have been investigated by Bazley and Montrol (18), and Northup and Hsu (19) have discussed the extension to multiple quantum transitions. Goody (6), however, suggests accepting eq. (53) simply as an experimental rather than a theoretical expression.

Information on collisional relaxation times is available only for a limited number of gases (20-26). For diatomic gases, an empirical relation is given by Millikan and White (22) as

$$P\eta = \exp[A(T^{-1/3}-0.015\mu^{1/4})-18.42] \tag{54}$$

Values of A and μ for carbon monoxide are A = 1.75 and μ = 14. Note that η decreases rapidly with increasing temperature.

B. EQUATION OF TRANSFER

The formulation of the equation of transfer for vibrational non-equilibrium is treated in detail by Goody (6), Gilles (27), Gilles and Vincenti (28), and Tiwari (29), and the complete derivation will not be repeated here. The formulation is based upon the assumption of a harmonic oscillator as well as two level transitions between vibrational states which restricts the analysis to fundamental bands. However, under conditions for which the assumption of LTE is not justified, combination and overtone bands do not contribute significantly to the radiative transfer process (29). When the assumption of LTE is valid, the equation of transfer reduces directly to the conventional macroscopic equation, and the restrictions to harmonic oscillation and two level transitions no longer apply.

Following Goody (6), the equation of transfer may be written as

$$\frac{dI_\omega}{ds} = \kappa_\omega(J_\omega - I_\omega) \tag{55}$$

where the source function, J_ω, is expressed by

$$J_\omega = B_\omega \frac{E_v}{E_v^*} \tag{56}$$

and B_ω denotes black-body intensity. For $E_v = E_v^*$, this of course reduces to the equation of transfer for LTE.

The important point concerning eq. (55) is that κ_ω is the equilibrium absorption coefficient; i.e., it corresponds to the local kinetic temperature. An explanation of this is given by Goody (6). More recently Gilles (27), and Gilles and Vincenti (28) have pointed out that this is strictly a low temperature approximation. At elevated temperatures, however, collisional relaxation is very rapid, and it is doubtful that physical situations exist at elevated temperatures for which non-LTE effects would be important.

For illustrative purposes, it will be convenient to temporarily restrict attention to diatomic gases, such that only a single fundamental band is considered. Under steady-state conditions, combination of eqs. (52), (53), and (55) yields

$$\left(\frac{E_v}{E_v^*}\right)\left[\frac{E_v^*}{\eta} + \int_0^{4\pi} d\Omega \int_0^\infty \kappa_\omega B_\omega d\omega\right] = \frac{E_v^*}{\eta} + \int_0^{4\pi} d\Omega \int_0^\infty \kappa_\omega I_\omega d\omega$$

Further, upon defining a time constant

$$\eta_r = \frac{E_v^*}{\int_0^{4\pi} d\Omega \int_0^\infty \kappa_\omega B_\omega d\omega} \tag{57}$$

the source function, J_ω, may now be written as

$$J_\omega = B_\omega \left[\frac{\eta_r + \eta X}{\eta_r + \eta}\right] \tag{58}$$

where

$$X = \frac{\int_0^{4\pi} d\Omega \int_0^{\infty} \kappa_\omega I_\omega d\omega}{\int_0^{4\pi} d\Omega \int_0^{\infty} \kappa_\omega B_\omega d\omega} \tag{59}$$

The time constant η_r is the radiative life time for vibrational states, and by assuming that, within the narrow band, B_W may be taken as independent of wave number, then it may be shown that (6)

$$1/\eta_r = 8\pi c \omega_o^2 (P/n) S(T) \tag{60}$$

where n is the molecular number density, ω_o is the wave number at the band center, and $S(T)$ is the band intensity. Employing the perfect gas law $P = nkT$, and since $S(T) \sim T^r$ for a fundamental band, it readily follows that the radiative life time is independent of both temperature and pressure.

Now, since B_ω and J_ω are isotropic and slowly varying functions of wave number within the band, then upon combining eqs. (51), (55), and (58), the nonequilibrium source function may be expressed as

$$J_{\omega_o} = B_{\omega_o} + \frac{1}{2} \left(\frac{\eta}{\eta_r}\right) H \tag{61}$$

where

$$H = - \frac{\int_0^{\infty} (dq_{R\omega}/dy) d\omega}{2\pi \int_0^{\infty} \kappa_\omega d\omega} \tag{62}$$

and J_{ω_o} and B_{ω_o} denote quantities evaluated at the band center.

Since $J_{\omega_o} = B_{\omega_o}$ for LTE, eq. (61) clearly illustrates that the degree of nonequilibrium is characeterized by the parameter η/η_r. When η/η_r is small, the source function J_{ω_o} reduces to the black body intensity B_{ω_o}, and the assumption of LTE is justified. On the other hand, in the limit of large η/η_r the divergence of the radiative flux becomes zero (6).

This physically corresponds to the situation for which vibrational transitions are radiatively controlled, such that all photons absorbed by the gas will in turn be re-emitted. There will thus be no net addition (or loss) of radiative energy to any gas element. For intermediate values of η/η_r, the divergence of the radiative flux will have a lower value than that corresponding to the condition of LTE. Consequently, the internal transfer of radiative energy within the gas will be reduced as the result of vibrational nonequilibrium. It is important to note from eqs. (61) and (62) that, regardless of the magnitude of η/η_r, the assumption of LTE is always justified for the case of radiative equilibrium (i.e., $dq_R/dy = 0$). This conclusion, of course, applies only for the present restriction of a gas having a single band. The preceding analysis may, however, easily be extended to multiple band spectra.

C. RADIATIVE FLUX EQUATION

The equation of transfer, eq. (55), may be integrated in the conventional manner so as to yield the expression for the spectral radiative flux, $q_{R\omega}$, with the result (30)

$$q_{R\omega} = 2B_{1\omega} E_3(\kappa_\omega y) - 2B_{2\omega} E_3[\kappa_\omega (L-y)] + 2\pi\{\int_0^y J_\omega(z)\kappa_\omega E_2[\kappa_\omega(y-z)]dz - \int_y^L J_\omega(z)\kappa_\omega E_2[\kappa_\omega(z-y)]dz\} \tag{63}$$

where $B_{1\omega}$ and $B_{2\omega}$ are the surface radiosities, while $E_n(x)$ is the exponential integral

$$E_n(x) = \int_0^1 \mu^{n-2} e^{-x/\mu} d\mu$$

The expressions for the surface radiosities are further given as (30)

$$B_{1\omega} = \varepsilon_{1\omega} e_{1\omega} + 2\,(1-\varepsilon_{1\omega})[B_{2\omega} E_3(\kappa_\omega L) + \pi \int_o^L J_\omega(z)\kappa_\omega E_2(\kappa_\omega z)dz] \tag{64a}$$

$$B_{2\omega} = \varepsilon_{2\omega} e_{2\omega} + 2\,(1-\varepsilon_{2\omega})[B_{1\omega} E_3(\kappa_\omega L) + \pi \int_o^L J_\omega(z)\kappa_\omega E_2(\kappa_\omega L-\kappa_\omega z)dz] \tag{64b}$$

The spectral absorption coefficient, κ_ω, has been taken to be independent of temperature in eqs. (63) and (64), and this effectively constitutes a linearization for small temperature differences. Note that for black surfaces $B_{1\omega} = e_{1\omega}$ and $B_{2\omega} = e_2$, whereas for LTE $J_\omega(y) = B_\omega(y) = e_\omega(y)/\pi$, with e_ω denoting Planck's function.

An often employed approximation in radiative transfer involves approximating the exponential integral $E_2(x)$ by an exponential function, such that $E_2(x) \simeq a\,\exp(-bx)$. Several combinations of a and b have been utilized, and for present purposes the approximation will be chosen as

$$E_2(x) \simeq \frac{3}{4}\exp(-\frac{3x}{2}) \tag{65a}$$

$$E_3(x) = -\int E_2(x)dx \simeq \frac{1}{2}\exp(-\frac{3x}{2}) \tag{65b}$$

The total radiative flux is further given by

$$q_R = \int_o^\infty q_{R\omega} d\omega \tag{66}$$

In the subsequent discussion, attention will be directed solely to black bounding surfaces, although surface emittance effects will be discussed in Section IV. Thus, upon combining eqs. (63), (65), and (66), the total radiative flux is given by

$$\begin{aligned} q_R = e_1 - e_2 &+ \frac{3}{2}\int_o^y [\pi J_{\omega_o}(z) - e_{1\omega_o}]\int_{\Delta\omega} \kappa_\omega \exp[-\frac{3}{2}\kappa_\omega(y-z)]d\omega dz \\ &- \frac{3}{2}\int_y^L [\pi J_{\omega_o}(z) - e_{2\omega_o}]\int_{\Delta\omega} \kappa_\omega \exp[-\frac{3}{2}\kappa_\omega(z-y)]d\omega dz \end{aligned} \tag{67}$$

where $e = \sigma T^4$, with σ denoting the Stefan-Bolizmann constant, while Aw indicates integration over the single band, again recalling that J_W and e_ω are slowly varying functions of wave number over the single band.

The primary motivation for employing the exponential kernel approximation in the present formulation is that it allows the kernel function in eq. (67) to be expressed in terms of the total band absorptance, since, from eq. (11)

$$\frac{dA}{dy} = A'(y) = \int_{\Delta\omega} \kappa_\omega \, e^{-\kappa_\omega y} \, d\omega$$

and this is the form of the kernel function in eq. (67). Thus, letting

$$\xi = \frac{y}{L} \quad , \quad u_o = \frac{SPL}{A_o}$$

and employing the dimensionless band absorptance, $\bar{A}(u,\beta)$, as defined by eq. (23), the final form of the radiative flux equation is obtained by combining eps. (61), (62), and (67) as

$$\begin{aligned} q_R(\xi) = e_1 - e_2 + \frac{3}{2} A_o u_o \{ & \int_o^\xi [e_{\omega_o}(\xi') - e_{1\omega_o}] \bar{A}'[\tfrac{3}{2} u_o(\xi - \xi')] d\xi' \\ & - \int_\xi^1 [e_{\omega_o}(\xi') - e_{2\omega_o}] \bar{A}'[\tfrac{3}{2} u_o(\xi' - \xi) d\xi' \} \\ & - \frac{3}{8} \left(\frac{\eta}{\eta_r}\right) \{ \int_o^\xi (dq_R/d\xi') \bar{A}'[\tfrac{3}{2} u_o(\xi - \xi')] d\xi' \\ & - \int_\xi^1 (dq_R/d\xi') \bar{A}'[\tfrac{3}{2} u_o(\xi' - \xi)] d\xi' \} \end{aligned} \tag{68}$$

where $\bar{A}'(u)$ denotes the derivative of $\bar{A}(u)$ with respect to u. Note that rotational line structure is included in eq. (68) through the band absorptance. Furthermore, eq. (68) describes the radiative flux for non-LTE in terms of the band absorptance for a gas in LTE. As previously discussed, following eq. (56), this is appropriate since κ_ω is an equilibrium absorption coefficient even under non-LTE conditions.

The non-LTE influence in eq. (68) is through the latter terms which are proportional to η/η_r, and which vanish in the limit of LTE (i.e., $\eta/\eta_r \to 0$). Although eq. (68) applies only to a single band spectrum; for LTE the extension to multiple bands requires simply a summation of the important bands. This will be illustrated in Section IV.

Equation (68) possesses two convenient limiting forms. One is the conventional optically thin limit, while the other, the large path length limit, corresponds to $u_o >> 1$, and for infrared radiation this limit differs considerably from the optically thick or Rosseland limit. These two limiting forms of eq. (68) will be treated in the following subsections.

D. OPTICALLY THIN LIMIT

As discussed by Sampson (31), the influence of non-LTE is most pronounced in the optically thin limit. Following Cess and Tiwari (32), this limit may be obtained by employing the linear limit for the band absorptance, eq. (43a), since the optically thin limit corresponds to $u_o << 1$. In the optically thin limit one is generally concerned with the divergence of the radiative flux (30), and upon differentiating eq. (68) and employing the linear limit $\bar{A}'(u) = 1$, then the appropriate expression for $u_o << 1$ becomes

$$-\frac{dq_R}{d\xi}\left(1 + \frac{3}{4}\frac{\eta}{\eta_r}\right) = 3A_o\, u_o\left[e_{\omega_o}(\xi) - e_{1\omega_o}\right] \tag{69}$$

An alternate approach to the optically thin limit is given in ref. (33), which does not make use of the exponential kernel approximation as given by eq. (65), and it is shown that the factor of 3 appearing on the right

side of eq. (69) is replaced by 4 in the exact formulation. Further comments on the application of the exponential kernel approximation to infrared radiative transfer are given by Grief and Habib (34).

It should be observed that eq. (69) is independent of rotational line structure, and this is consistent with the previous discussion on the invariance of $\bar{A}(u,\beta)$ with the line structure parameter β in the linear limit. The obvious simplification of the non-LTE influence in eq. (69) should also be noted. As such, all optically thin analyses based on the assumption of LTE may be modified to include the effect of non-LTE simply by multiplying the divergence of the radiative flux by a constant involving the nonequilibrium parameter η/η_r.

E. LARGE PATH LENGTH LIMIT

Even though the optically thick (Rosseland) limit does not apply to vibration-rotation bands, since optically nonthick radiation will always occur in the band wings (33, 35), a large path length limit does exist and is achieved for $u_o >> 1$. Employing the method of steepest descent, it may be shown that the asymptotic form of the integrals appearing in eq. (68) corresponds to the use of the logarithmic limit for the band absorptance, eq. (43c). For illustrative purposes it will again be convenient to treat the divergence of the radiative flux vector. Thus, upon differentiating eq. (68), performing a subsequent integration by parts, and utilizing the asymptotic formulation $\bar{A}(u) = \ln u$, one obtains

$$\frac{dq_R}{d\xi} = A_o \int_o^1 \frac{de_{\omega_o}}{d\xi'} \frac{d\xi'}{\xi-\xi'} + \frac{1}{4u_o}\left(\frac{\eta}{\eta_r}\right) \int_o^1 \frac{dq_R}{d\xi'} \frac{d\xi'}{(\xi-\xi')^2} \tag{70}$$

In arriving at eq. (70), continuity of temperature has been assumed

between the gas and the bounding surfaces. This is physically realistic, since $u_o >> 1$ implies that the central portion of the band is optically thick, which would insure temperature continuity. A more quantitative treatment of this point will be given in Section IV.

Since the large path length limit is an asymptotic limit for large u_o, it readily follows that the second term in eq. (70) may be deleted, with the result that

$$\frac{dq_R}{d\xi} = A_o \int_o^1 \frac{d\xi'}{\xi - \xi'} \tag{71}$$

and this is precisely the result for LTE. The vanishing of the non-LTE influence in this limit can further be illustrated by consideration of the source function. As previously discussed, non-LTE effects enter solely through the source function, and from eq. (61) this may be expressed as

$$J_{\omega_o}(\xi) = \frac{e_{\omega_o}(\xi)}{\pi} - \frac{1}{4\pi u_o A_o}\left(\frac{\eta}{\eta_r}\right)\frac{dq_R}{d\xi} \tag{72}$$

Employing eq. (70) and taking the limit for large u_o yields to result that $J_{\omega_o}(\xi) = e_{\omega_o}(\xi)/\pi$, which is the source function for LTE. In the large path length limit, optically thick radiation occurs in the central portion of the band, whereas the wing regions constitute a continuous transition from optically thick to optically thin radiation. Vibrational energy levels are evidently dominated by the optically thick portion of the spectrum, which suppresses non-LTE effects (31), such that this is the reason for the existence of LTE in the large path length limit.

A second significant simplification associated with eq. (71) is that, as for the optically thin limit, the radiative transfer process is

independent of line structure, since the line structure parameter does not appear in the equation. The reason for this is that the band absorptance becomes invariant with line structure for large u_o, and it is this asymptotic result for the band absorptance which yields eq. (71). Note also that eq. (71) is independent of both pressure and band intensity, and this will be discussed in more detail in Section IV.

IV. RADIATIVE TRANSFER ANALYSES

This section presents several analyses illustrating the application of conservation of energy to the determination of the temperature profile within an infrared radiating gas, with primary emphasis upon the basic features of the radiative transfer process. For this purpose, simple illustrative physical models will be considered. Referring to the coordinate system of Fig. 6, Sections IV-A, IV-B, and IV-C consider the symmetric case for which $T_2 = T_1$ and there is a uniform heat source per unit volume, Q, within the gas. In Section IV-A, radiative transfer is assumed to be the sole mechanism of energy transfer through the gas, such that the energy equation constitutes a balance between the divergence of the radiative flux and the source Q. The same situation is considered in Section IV-B, except that molecular conduction is included as an energy transfer mechanism in order to illustrate the relative importance of conduction versus radiation within the gas. In both these sections restriction is made to LTE, while the influence of vibrational nonequilibrium is treated in Section IV-C. A brief discussion of radiative equilibrium is included in Section IV-D for purposes of illustrating a physical system which is not symmetric.

A. RADIATIVE TRANSFER

The first illustrative solution is that for which radiative transfer is the sole mechanism of energy transfer within the gas. The local temperature distribution is thus a consequence of the uniform heat source, Q, adding energy to the gas which in turn is transferred through the gas to the bounding surfaces by radiative transfer. The two bounding

surfaces are assumed to be at the same temperature, $T_2 = T_1$, LTE is assumed to prevail, and for the time being the bounding surfaces are taken to be black.

The energy equation for this situation is

$$\frac{dq_R}{dy} = Q$$

and since the problem is symmetric, then

$$q_R = \frac{QL}{2}(2\xi - 1) \tag{73}$$

where again $\xi = y/L$. For a single-band spectrum, the radiative flux is described by eq. (68). As previously discussed, however, when LTE prevails eq. (68) may be extended to multiple band spectra by summing eq. (68) over the individual bands. Furthermore, since small temperature differences have been assumed in arriving at eq. (68), one may additionally employ the linearization

$$e_{\omega_i} - e_{1\omega_i} \quad (\frac{de_{\omega_i}}{dT})_{T_1} (T-T_1) \tag{74}$$

where the subscript i refers to the ith band, such that ω_i is the wave number location of the band. The subsequent extension of eq. (68) thus yields

$$q_R = \frac{3}{2} \sum_{i=1}^{n} A_{oi} \omega_{oi} (\frac{de_{\omega_i}}{dT})_{T_1}]\{\int_o^{\xi} [T(\xi')-T_1]\bar{A}'[\frac{3}{2}u_{oi}(\xi-\xi')]d\xi' - \int_{\xi}^{1} [T(\xi')-T_1]\bar{A}'[\frac{3}{2}u_{oi}(\xi'-\xi)]d\xi'\} \tag{75}$$

where n represents the number of vibration-rotation bands in the spectrum.

Upon combining eqs. (73) and (75), conservation of energy is described

by the integral equation

$$\xi - \frac{1}{2} = \frac{3}{2} \sum_{i=1}^{n} \left(\frac{H_i u_{oi}}{H}\right)\left\{\int_0^{\xi} \phi(\xi')\bar{A}'\left[\frac{3u_{oi}}{2}(\xi-\xi')\right]d\xi' - \int_{\xi}^{1} \phi(\xi')\bar{A}'\left[\frac{3u_{oi}}{2}(\xi'-\xi)\right]d\xi'\right\} \tag{76}$$

where

$$H_i = A_{oi}\left(\frac{de_{\omega_i}}{dT}\right)_{T_1} \tag{77a}$$

$$H = \sum_{i=1}^{n} H_i \tag{77b}$$

$$\phi = \frac{T-T_1}{QL/H} \tag{77c}$$

Employing the band absorptance correlation of Tien and Lowder (11), as expressed by eq. (45), together with the empirical correlations for $S_i(T)$, $A_{oi}(T)$, and $\beta_1(T,P_e)$ given by Edwards, et al (10), eq. (76) was solved numerically for CO_2, H_2O, and CH_4 (35). These solutions were obtained by the method of undetermined parameters, in which a polynomial solution for $\phi(\xi)$ is assumed and the constants evaluated by satisfying the integral equation at equally spaced locations. Both quadratic and quartic solutions were utilized, with the two solutions yielding virtually identical results. Before discussing these results, however, it will be convenient to first investigate the optically thin and large path length solutions.

1. Optically Thin Solution

Following Section III-D, the optically thin solution to eq. (76) is achieved by letting $\bar{A}'(u) = 1$, and it readily follows from eq. (76) that

$$\phi = \frac{H}{3\sum_{i=1}^{n} H_i u_{oi}}$$

or

$$T - T_1 = \frac{Q}{3P\sum_{i=1}^{n} S_i(T_1)(de_{\omega_i}/dT)_{T_1}} \tag{78}$$

The fact that eq. (78) predicts the gas temperature to be independent of location is consistent with the result that in optically thin limit each gas element exchanges radiation directly with the bounding surfaces, and this exchange process is thus independent of position (30).

As discussed in Section III-D, eq. (78) is independent of the line structure parameter β_i. One may further note that the optically thin limit is also independent of the band width parameter A_{oi}. An indication of the relative ability of gases to transfer radiative energy is clearly given by eq. (78), since a lower gas temperature implies a greater capability to transmit energy. Thus, the appropriate gas property that serves to measure the ability of a gas to radiative energy is the quantity[4]

$$K = \sum_{i=1}^{n} S_i(T)(de_{\omega_i}/dT) \tag{79}$$

For example, CO_2 has a larger value of K than does H_2O, and thus CO_2 will have the greatest ability of transferring radiative energy in the optically thin limit.

2. Large Path Length Limit

As discussed in Section III-E, the large path length limit is achieved

[4]The quantity K may be related to the linearized Planck mean coefficient, as defined by Goody (6), and Cogley, Vincenti, and Gilles (36).

when $u_{oi} >> 1$ for each band of importance, and this limit corresponds to employing $\bar{A}'(u) = 1/u$ in eq. (76), with the result that

$$\xi - \frac{1}{2} = \int_0^1 \phi(\xi') \frac{d\xi'}{\xi - \xi'} \qquad (80$$

Aside from the obvious simplification in form in going from eq. (76) to (80), there are other more striking consequences associated with eq. (80). For example, of the three correlation quantities A_{oi}, β_i, and S_i, only A_{oi} appears in eq. (80) through the definition of $\phi(\xi)$. The dependence upon this single correlation quantity in the large path length limit has also been illustrated by Edwards; et al"(10) in dealing with laminar flow between parallel plates. The absence of the line structure parameter β_i bas been discussed in Section III-E, while the invariance of the band absorptance S_i is physically logical, since the central portion of the band is saturated in the large path length limit, and consequently the radiative transfer process should not depend upon the total band area.

A further simplification associated with eq. (80) is that the temperature profile within the gas is independent of pressure. This is not the case with respect to the general formulation, eq. (76), for which pressure appears both in the dimensionless path length u_{oi} and in the line structure parameter β_i. This invariance of temperature profile with pressure can also be found from the results of Edwards, et al (10), and experimental confirmation has recently been presented by Schimmel, Novotny, and Olsofka (37).

Equation (80) constitutes a singular integral equation with a Cauchy type kernel, for which the solution is (38)

$$\phi(\xi) = \frac{1}{\pi} [\xi(1-\xi)]^{1/2} + C[\xi(1-\xi)]^{-1/2}$$

where C is an arbitrary constant which arises since the solution of eq. (80) is not unique. However, to satisfy the physical requirement of finite temperature everywhere within the gas, C = 0, and

$$\phi(\xi) = \frac{1}{\pi} [\xi(1-\xi)]^{1/2} \tag{81}$$

Note that this temperature profile yields the result that the gas temperature at a surface is equal to the surface temperature, and this absence of a temperature slip is characteristic of optically thick radiation (30). As discussed in Section III-E, this is a consequence of the fact that optically thick radiation is occurring in certain spectral regions. Optically nonthick radiation exists, however, in other spectral regions (33), with the result that eq. (81) differs substantially from the temperature profile which would be predicted using a Rosseland type (or diffusion) equation.

Upon recasting eq. (81) as

$$T - T_1 = \frac{QL}{\pi H} [\xi(1-\xi)]^{1/2}$$

it is apparent that the gas property which measures the ability of a gas to transfer radiative energy in the large path length limit is

$$H = \sum_{i=1}^{n} A_{oi} \left(\frac{de_{\omega_i}}{dT}\right) \tag{82}$$

as opposed to the optically thin transport property K, defined by eq. (79).

3. Results

For the sake of brevity, numerical solutions to eq. (76) will be presented solely in terms of the centerline temperature; i.e.,

$T_c = T(\xi = 1/2)$. In the case of a single-band gas, the summation sign is removed in eq. (76) and results may be expressed in terms of the single pair of parameters u_o and β. This is illustrated by the solid curves in Fig. 7, and the results apply to any situation for which radiative transfer within the gas is the result of a single band. For small u_o the results approach the optically thin limit as described by eq. (78). The maximum influence of the line structure parameter exists for intermediate values of u_o, while in the large path length limit the solution again becomes independent of β.

Also illustrated in Fig. 7 is a solution employing the box model, for which a constant absorption coefficient $\bar{\kappa}$ is assumed within a finite band width ω. The relation between this width and the bandwidth parameter A_o was taken to be $\omega = (214/38)\, A_o$, which is appropriate for CO (33), and the value of the mean coefficient is in turn $\bar{\kappa} = SP/\Delta\omega$. Clearly, such a model does not account for line structure. Since the box model preserves the band intensity, it reduces to the correct optically thin limit, but a significant departure between the two solutions takes place for increasing u_o. This is easily explained on physical grounds. In the central portion of the band the box model underpredicts the value of the spectral absorption coefficient, and it thus will yield optically thin results for greater values of u_o than will the solution employing the band absorptance. At large values of u_o the box model overpredicts the centerline temperature due to the neglect of the band wings. For large path lengths the wing regions contribute primarily to radiative transfer. Since the box model neglects the wings, it underestimates the ability of the gas to transfer radiant energy for large u_o values, and consequently it overpredicts the centerline temperature.

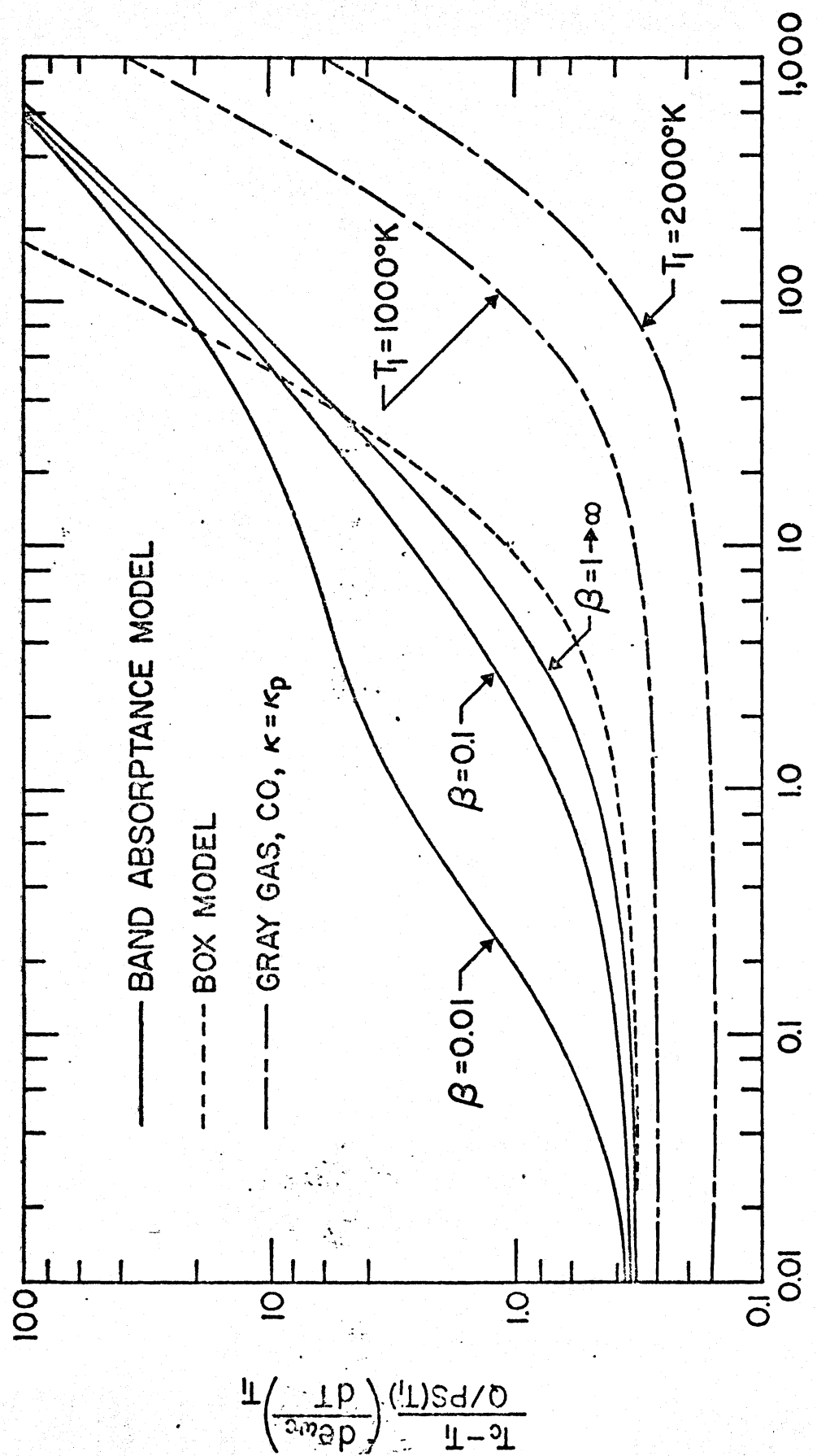

Fig. 7. Comparison of results for a single band gas.

The inapplicability of the optically thick (or Rosseland) limit should again be emphasized. From the box model, it readily follows that $(T_c-T_1) \sim L^2$ for large u_o (33), and this corresponds to optically thick radiation occurring throughout the finite width band. From the large path length solution of eq. (81), however, $(T_c-T_1) \sim L$, such that the occurrence of nonthick radiation within the band wings significantly influences the nature of the radiative transfer process for large u_o.

Also shown in Fig. 7 are gray gas results (33), where, for lack of a more rational choice, the mean absorption coefficient has been chosen as the Planck mean coefficient, which is defined as

$$\kappa_P = \frac{\int_o^\infty \kappa_\omega e_\omega(T)d\omega}{\sigma T^4} .$$

Specific comparisons are made for CO. It is quite obvious that the gray solution constitutes a rather large departure from reality.

With respect to multiple band spectra, dimensionless centerline temperatures for CO_2, H_2O, and CH_4, as obtained from eq. (76), are illustrated in Figs. 8 through 11. Since the abscissa variable is the pressure path length, the separate influence of pressure upon the centerline temperature is due solely to the alteration of the line structure of the bands due to pressure broadening. As the pressure is increased, the discrete line structure is eliminated, and, as illustrated in Figs. 8 through 11, pressure ceases to be a separate parameter in the high pressure limit. This of course is analogous to the large β limit of Fig. 7.

In the large path length limit, the dimensionless centerline temperature follows from eq. (81) to be

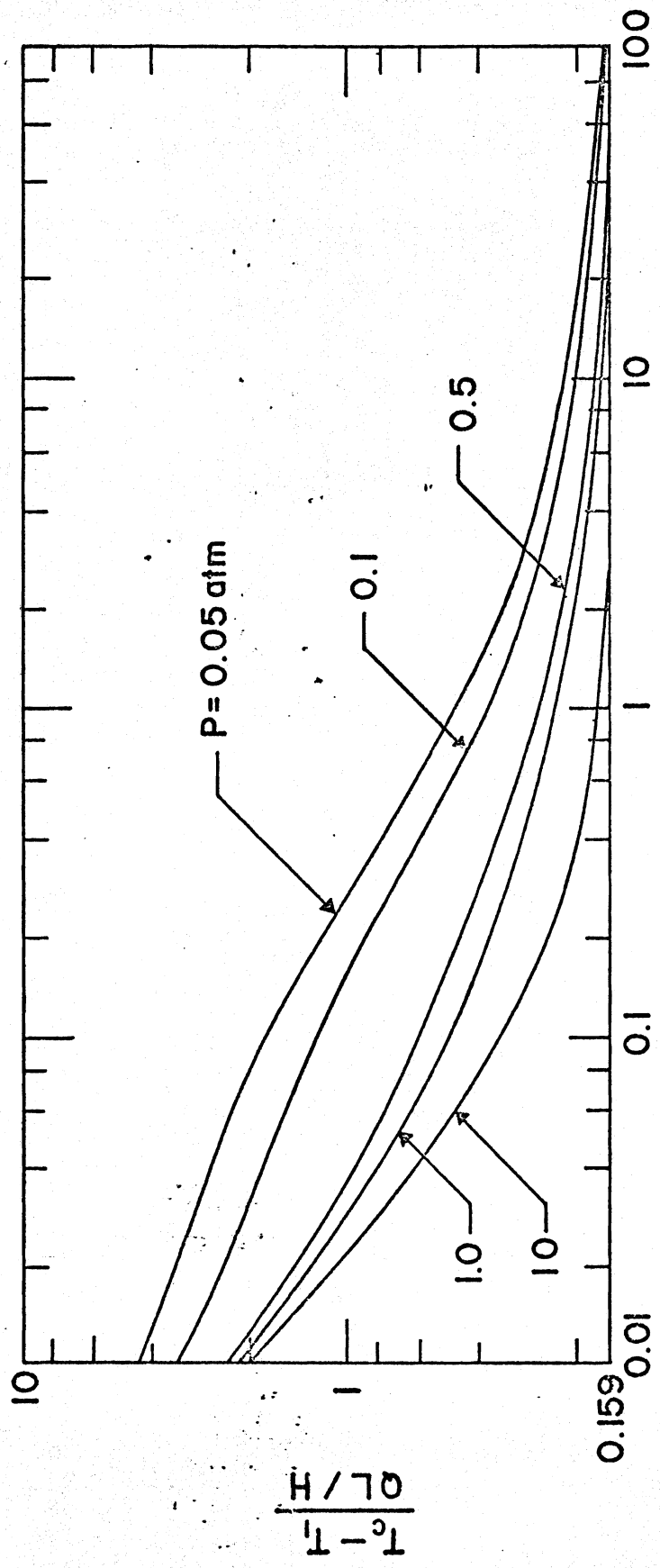

Fig. 8. Centerline temperature results for CO_2 with T_1 = 300°K.

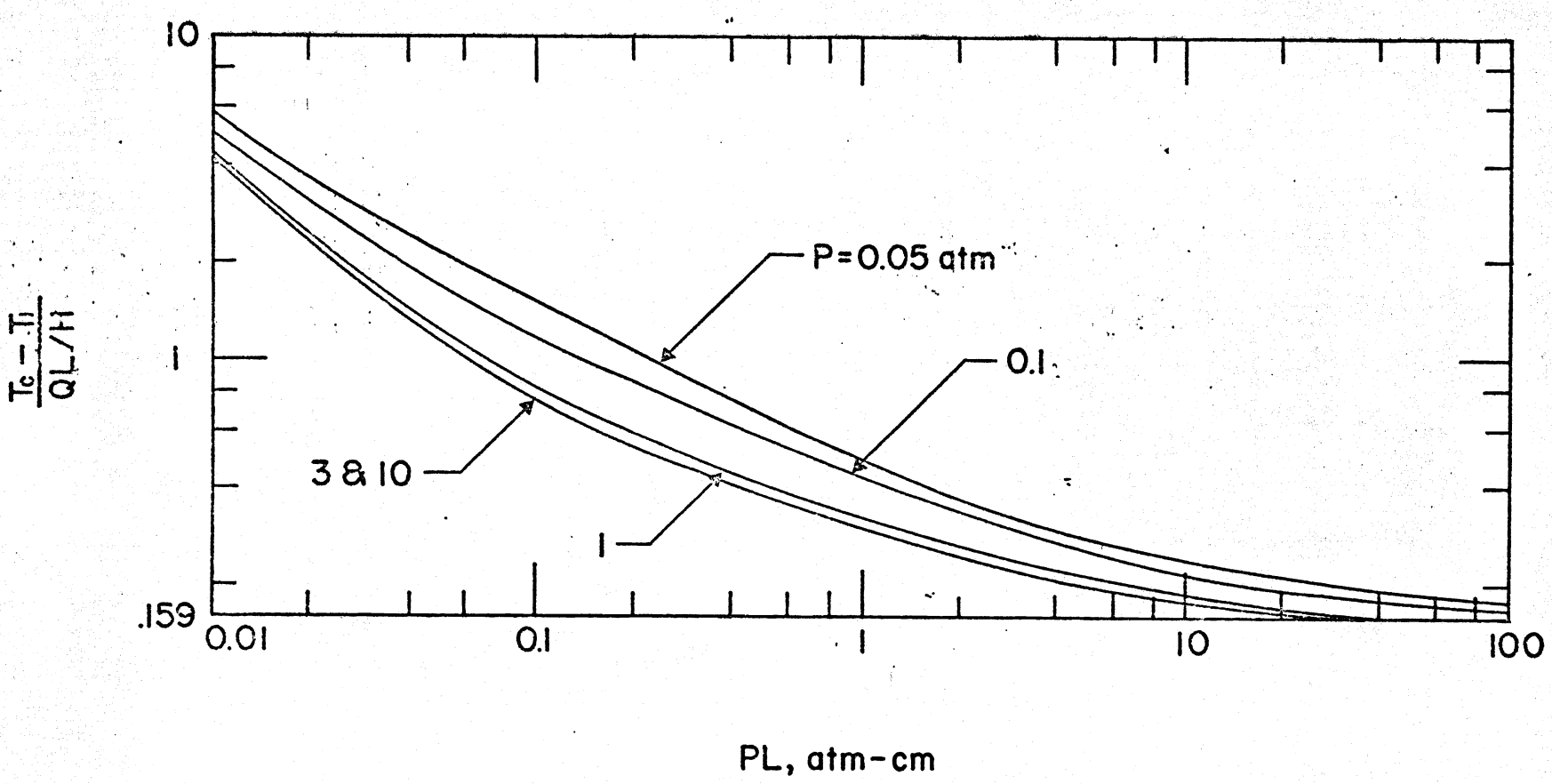

Fig. 9. Centerline temperature results for CO_2 with T_1 = 1,000°K.

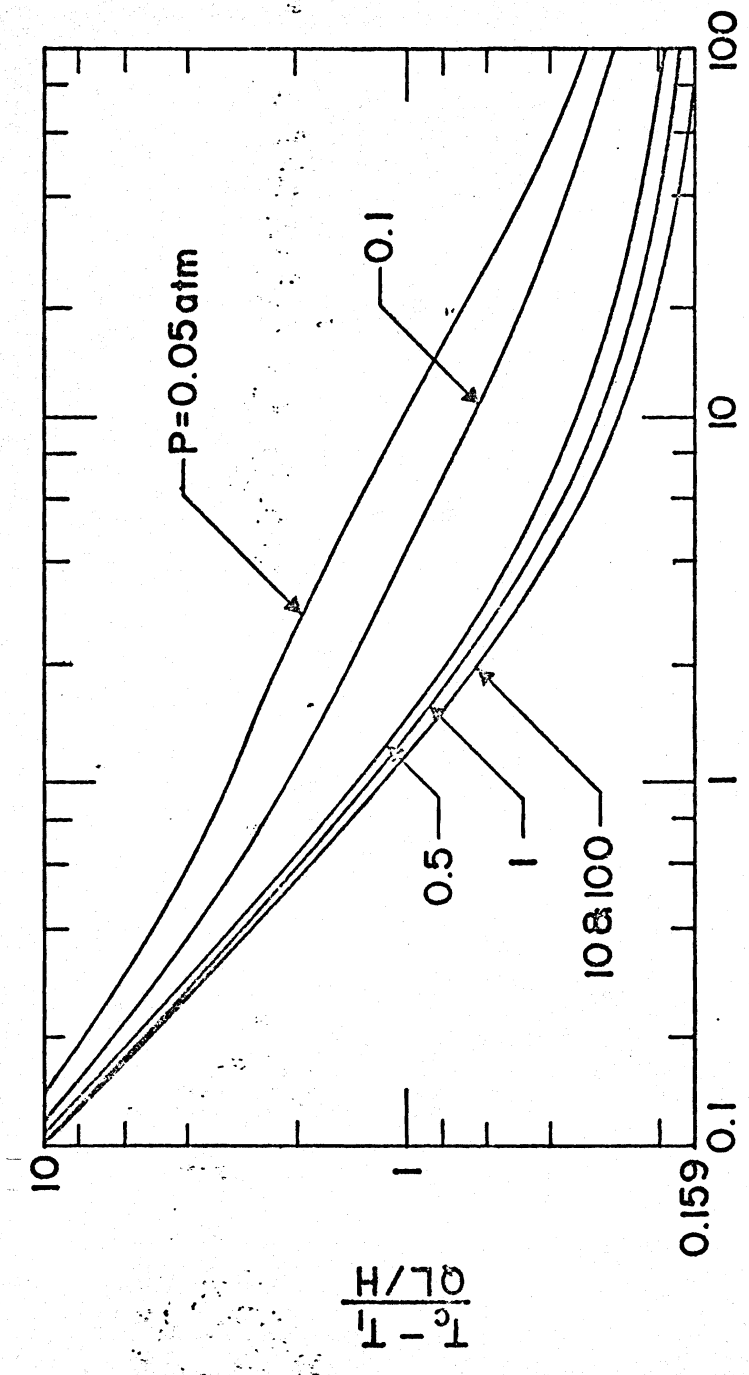

Fig. 10. Centerline temperature results for H_2O with T_1 = 1,000°K.

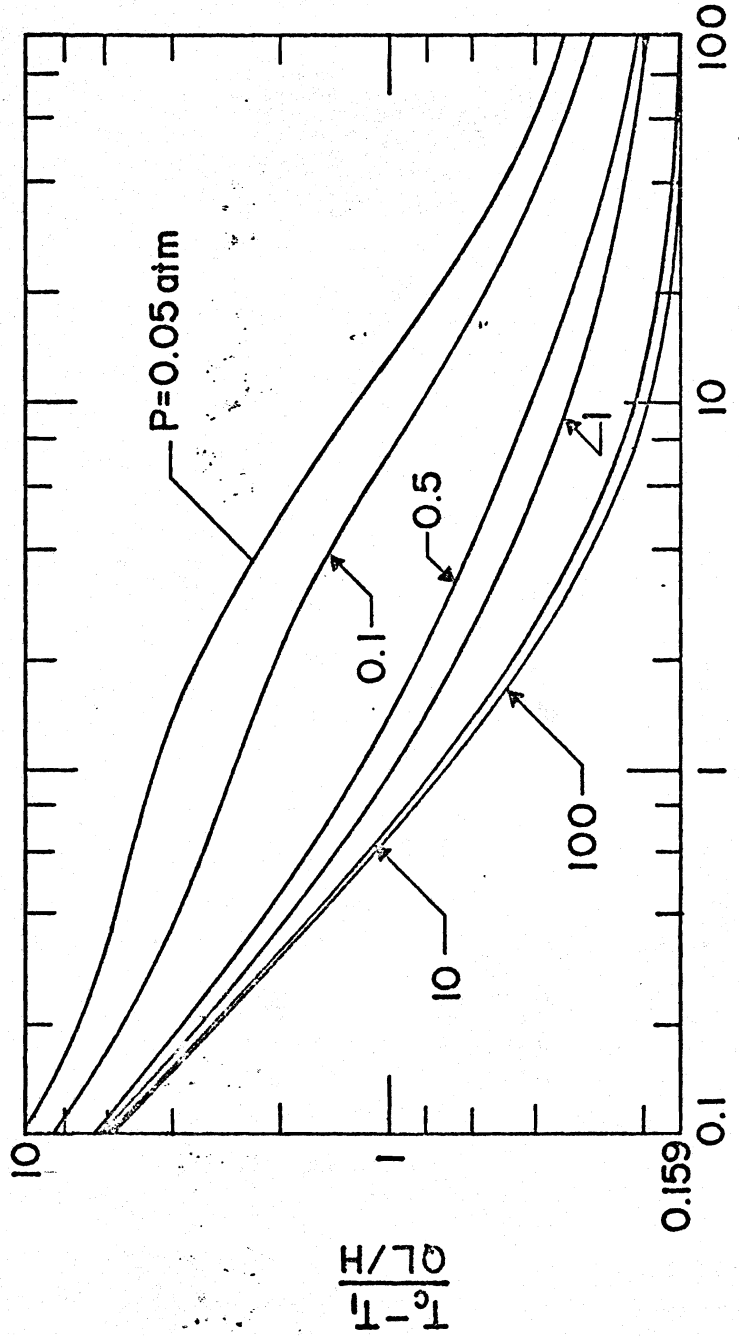

Fig. 11. Centerline temperature results for CH_4 with T_1 = 1,000°K.

$$\frac{T_c - T_1}{QL/H} = \frac{1}{2\pi} = 0.159 \qquad (83)$$

Figures 8 through 11 consequently serve to illustrate the conditions under which the large path length limit constitutes a useful means of describing the radiative transfer process. Although these figures correspond to a specific physical problem, the limits of applicability of the large path length limit should be qualitatively indicative of other physical situations. Additional numerical results are given by Cess and Tiwari (35).

A comparison of the relative ability of various gases to transmit radiative energy may be obtained by comparing the dimensional quantity $(T_c - T_1)/QL$. This is shown in Fig. 12 for a temperature of 500°K and a pressure of 1 atm. Recall that a lower centerline temperature implies a greater ability of the gas to transmit radiative energy, and that in the optically thin limit the radiative transfer capability of a given gas is dependent upon the magnitude of K given by eq. (79). For the four gases considered, CO_2 has the largest value of K, followed respectively by H_2O, CH_4, and CO. This is consistent with the results shown in Fig. 12 for small path lengths, i.e., CO_2 has the lowest centerline temperature, etc. As the path length is increased, however, CO_2 undergoes a transition from the most capable to nearly the least capable transmitter of radiative energy, since CO_2 has a small relative value for H, as defined by eq. (82), indicating that it is a poor radiator for large path lengths.

With respect to gases other than those considered here, the large path length property H may be evaluated solely from knowledge of the appropriate band locations and rotational constants by employing eqs. (30) and (82).

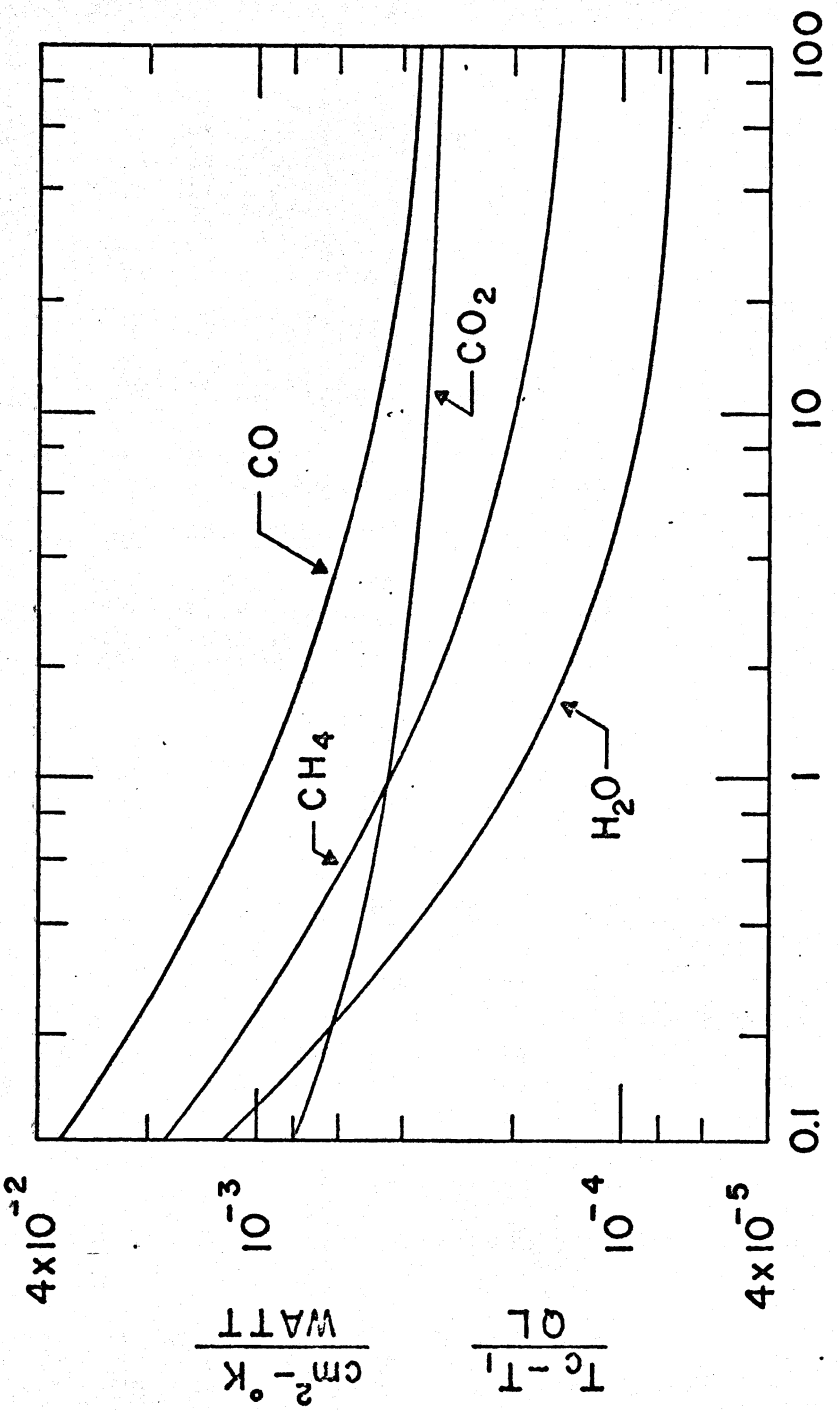

Fig. 12. Comparative results for P = 1 atm and T_1 = 500°K.

It should be emphasized that the large path length limit, as treated here, is not an exact asymptotic limit, since it makes use of the logarithmic asymptote for the band absorptance, which in itself is an approximate limiting expression.

4. Effect of Surface Emittance

The effect of nonblack surfaces upon infrared radiative transfer will now be investigated, utilizing the same physical model as previously considered. Restriction will, however, be made to single-band gases, so that this constitutes an extension of the results of Fig. 7. Both surfaces are assumed to have the same emittance, ε, and it is not necessary to postulate gray surfaces, since ε may be regarded as the spectral emittance at the wave number of the single band.

following Tiwari and Cess (39), the combination of eqs. (63) and (64), under the condition of LTE, yields

$$\begin{aligned}(\xi-1/2)\,\frac{2}{3u_o} = {} & \int_o^{\xi} \phi(\xi')\bar{A}'\left[\frac{3u_o}{2}(\xi-\xi')\right]d\xi' \\ & - \int_{\xi}^{1} \phi(\xi')\bar{A}'\left[\frac{3u_o}{2}(\xi'-\xi)\right]d\xi' \\ & + \int_o^{1} \phi(\xi')\sum_{m=o}^{\infty}(1-\varepsilon)^{m+1}\left\{\bar{A}'\left[\frac{3u_o}{2}(\xi'+\xi+m)\right]\right. \\ & \left. - \bar{A}'\left[\frac{3u_o}{2}(\xi'-\xi+1+m)\right]\right\}d\xi'\end{aligned} \tag{84}$$

as the appropriate energy equation. This of course reduces to the single band form of eq. (76) for $\varepsilon = 1$.

Numerical solutions of eq. (84) are available (39), and the dimensionless centerline temperature is illustrated in Fig. 13 for $\beta =$ [illegible]. As should be expected, a reduction in surface emittance gives rise to a higher

centerline temperature, since a lower surface emittance corresponds to a reduction in the energy transfer capability between the gas and the surfaces.

The optically thin limit readily follows from eq. (84) to be

$$\phi(\xi) = \frac{1}{3u_o}$$

and this coincides with the single-band form of eq. (78) for black surfaces. The invariance of surface emittance upon gas temperature is also observed for a gray gas under optically thin conditions (40). To explain this, recall that under optically thin conditions the surface radiosity is evaluated as if the gas were completely transparent (30), and since this corresponds to an isothermal enclosure for the present problem, the surface radiosity is equal to black body radiation irrespective of the value of the surface emittance.

In the large path length limit, eq. (84) reduces to

$$\xi - 1/2 = \int_o^1 \phi(\xi') \frac{d\xi'}{5-5'} + \int_o^1 \phi(\xi') \sum_{m=o}^{\infty} (1-\epsilon)^{m+1} \left[\frac{1}{(\xi'+\xi+m)} - \frac{1}{(\xi'-\xi+1+m)}\right] d\xi'$$

The solution to this equation is also illustrated in Fig. 13, and note that this limit does depend upon the surface emittance. On the other hand, for a gray gas or any gas with a nonvanishing absorption coefficient over the entire spectrum, the radiation in the optically thick (Rosseland) limit is independent of surface emittance (30, 41). With reference to the psesent large path length solution, it is radiation occurring in the band wings which is neither optically thin nor optically thick that produces the influence of ϵ upon the temperature profile within the gas.

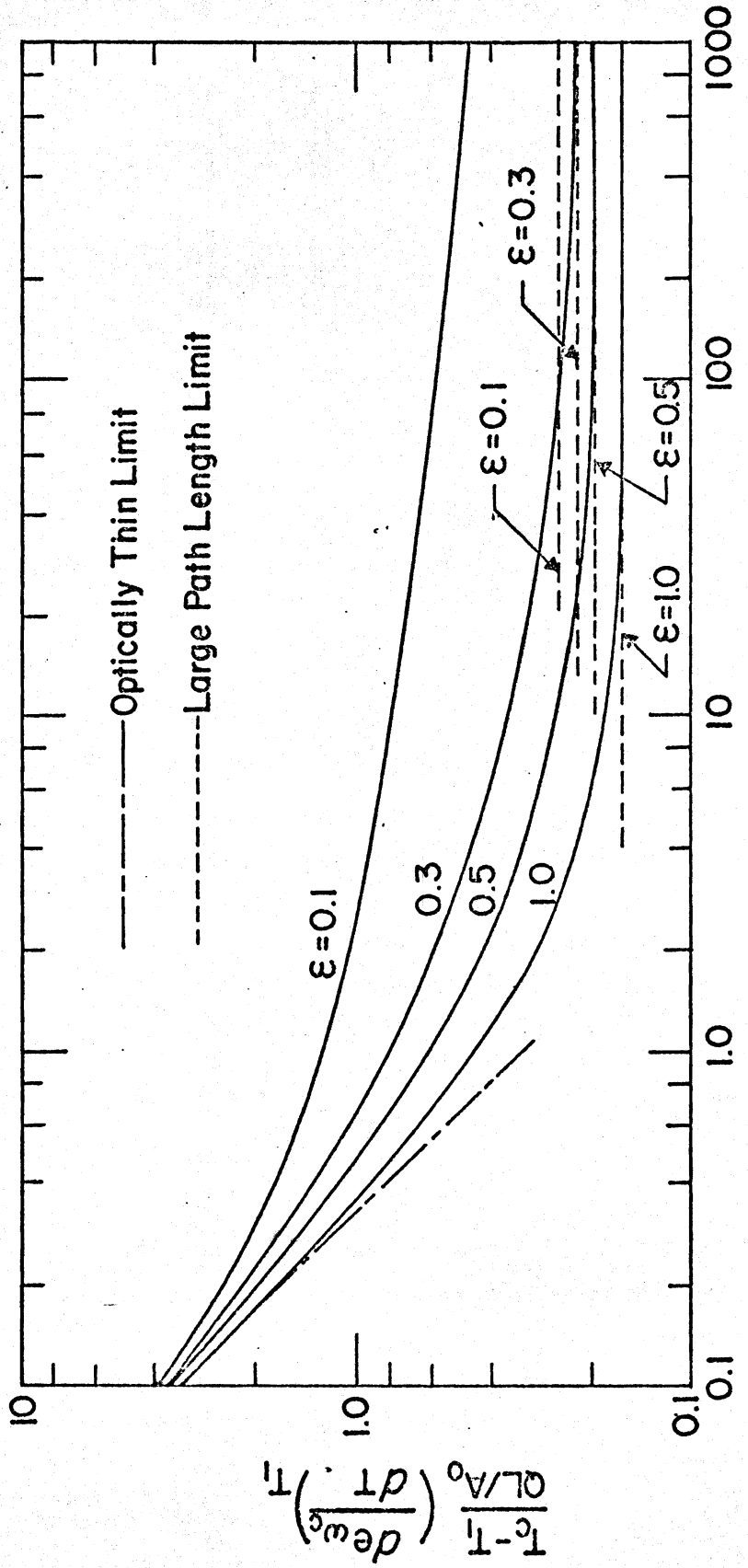

Fig. 13. Effect of surface emittance for a single band gas with $\beta = \infty$.

It may further be noted from Fig. 13 that as ε is decreased, the range of applicability of the limiting solutions are appreciably reduced. In particular, for $\varepsilon = 0.1$ an extremely large value of u_o would be required in order to approach the large u_o limit.

B. RADIATION-CONDUCTION INTERACTION

With the exception of atmospheric applications, molecular conduction within a gas must be regarded as a possible energy transport mechanism, and, in fact, for small physical dimensions it will dominate radiative transfer. The purpose of this subsection is to investigate the relative importance of radiation versus conduction as energy transport mechanisms, and the physical model of Section IV-A is again employed for illustrative purposes.

From conservation of energy, the temperature profile within the gas is described by

$$\lambda \frac{d^2T}{dy^2} - \frac{dq_R}{dy} + Q = 0$$

where λ is the thermal conductivity of the gas. Upon integrating this equation once, and noting that $dT/dy = 0$ and $q_R = 0$ for $y = L/2$, then

$$q_R = \lambda \frac{dT}{dy} + Q(y-L/2) \tag{85}$$

For a gas containing n vibration-rotation bands, the radiative flux is again described by eq. (75), such that eq. (85) yields the introdifferential equation

$$\frac{d\Theta}{d\xi} + \xi - 1/2 = \frac{3L}{2\lambda} \sum_{i=1}^{n} H_i u_{oi} \{ \int_o^{\xi} \Theta(\xi') \bar{A}' [\frac{3u_{oi}}{2} (\xi-\xi')] d\xi' - \int_{\xi}^{1} \Theta(\xi') \bar{A}' [\frac{3u_{oi}}{2} (\xi'-\xi)] d\xi' \} \tag{86}$$

where

$$\theta = \frac{T-T_1}{QL^2/\lambda}$$

and the quantity H_i is defined by eq. (77a). Since the presence of conduction implies continuity of temperature at the boundaries, the boundary condition for this equation is $\theta(0) = 0$. When radiative transfer within the gas is negligible, the solution of eq. (86) follows to be

$$\theta = \frac{1}{2}(\xi-\xi^2) \tag{87}$$

In the optically thin limit ($u_{oi} << 1$), eq. (86) may be expressed as

$$\frac{d^2\theta}{d\xi^2} - 3N\theta = -1 \tag{88}$$

subject to the boundary conditions

$$\theta(0) = 0, \quad \theta'(1/2) = 0$$

and for which

$$N = \frac{PL^2}{\lambda} \sum_{i=1} S_i(T_1)\left(\frac{de_{\omega_i}}{dT}\right)_{T_1} \tag{89}$$

Equation (88) possesses an elementary solution, from which the centerline temperature is found to be

$$\frac{T_c-T_1}{QL^2/\lambda} = \frac{1}{3N}\left\{1-2\left[\frac{\exp(-\frac{1}{2}\sqrt{3N})}{1+\exp(-\sqrt{3N})}\right]\right\}$$

It readily follows that the dimensionless gas property N characterizes the relative importance of radiation versus conduction within the gas under optically thin conditions. For particular values of P and L, it is actually the dimensional quantity

$$\frac{N}{PL^2} = \frac{1}{\lambda} \sum_{i=1}^{n} S_i \frac{de_{\omega_i}}{dT} \tag{90}$$

which characterizes this relative importance, and values of N/PL^2 are illustrated in Fig. 14. For CO, CO_2, H_2O, and CH_4, eq. (90) was evaluated employing the band intensities of Edwards, et al (10), while for N_2O and NH_3 the intensities where taken from Tien (1). The appropriate thermal conductivity values are from Tsederberg (42). It should again be emphasized that N/PL^2 characterizes radiation-conduction interaction only in the optically thin limit.

For the large path length limit ($u_{oi} >> 1$), eq. (86) reduces to

$$\frac{d\Theta}{d\xi} + \xi - 1/2 = M\int_0^1 \Theta(\xi') \frac{d\xi'}{\xi - \xi'} \tag{91}$$

where $\Theta(0) = 0$ is again the appropriate boundary condition, and

$$M = \frac{HL}{\lambda} = \frac{L}{\lambda} \sum_{i=1}^{n} A_{oi} \left(\frac{di}{dT}\right)_{T_1} \tag{92}$$

The dimensionless parameter M constitutes the radiation-conduction interaction parameter for the large path length limit, and the dimensional quantity M/L is illustrated in Fig. 15. For CO, CO_2, H_2O, and CH_4, this quantity was evaluated by using the A_{oi} values of Edwards, et al (10), while for N_2O and NH_3 the A_{oi} values were calculated from eq. (44).

A comparison of Figs. 14 and 15 shows a considerable difference in the radiation-conduction interaction for the optically thin limit as opposed to the large path length limit. For example, in the optically thin limit CO_2 possesses a large radiation interaction relative to the other gases, while the reverse is true in the large path length limit. On the other hand, just the opposite trend is

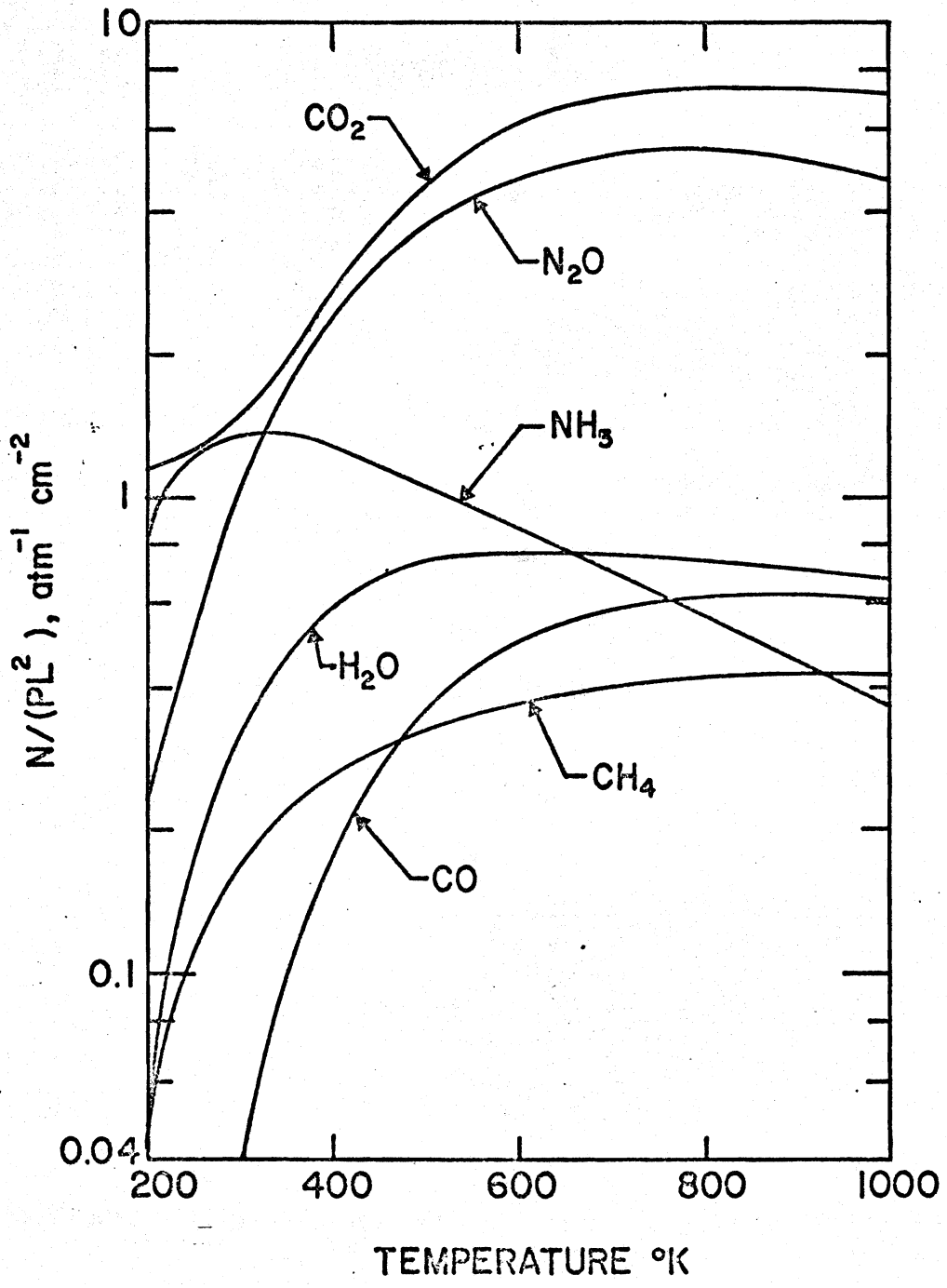

Fig. 14. Conduction-radiation interaction parameter for optically thin radiation.

observed for H_2O. Since the thermal conductivities of the various gases do not differ appreciably, this behavior is due to differences in radiative transfer in the optically thin and large path length limits, and a discussion to this effect has been given in Section IV-A.

Equation (91) does not appear to possess a closed form solution. A numerical solution has thus been obtained, and the dimensionless centerline temperature is illustrated in Fig. 16.

Numerical solutions of eq. (86), which is applicable for all u_{oi} values, have been obtained for several gases (32), and certain of these results are illustrated in Figs.. 17 through 19 for CO_2 and H_2O. The large path length limit, as given by Fig. 16, is also shown. From eq. (87), the centerline temperature for pure conduction follows to be

$$\frac{T_c - T_1}{QL^2/\lambda} = 0.125$$

and thus Figs. 17 through 19 serve to illustrate the influence of radiative transfer upon the temperature profile within the gas. As would be expected, the importance of radiation becomes more pronounced as the plate spacing is increased.

For the sake of brevity, comparisons involving the optically thin limit will be made only for CO_2 at a pressure of one atmosphere. These are illustrated in Figs. 20 and 21 for wall temperatures of 500°K and 1,000°K, respectively. In Fig. 20 it is evident that, when radiation is of importance, the radiative transfer process very nearly corresponds to the large path length limit. Conversely, this indicates that when the radiation is optically thin, it is in turn negligible relative to conduction, such that the optically thin limit does not constitute a useful limiting solution for the conditions illustrated in Fig. 20. This is

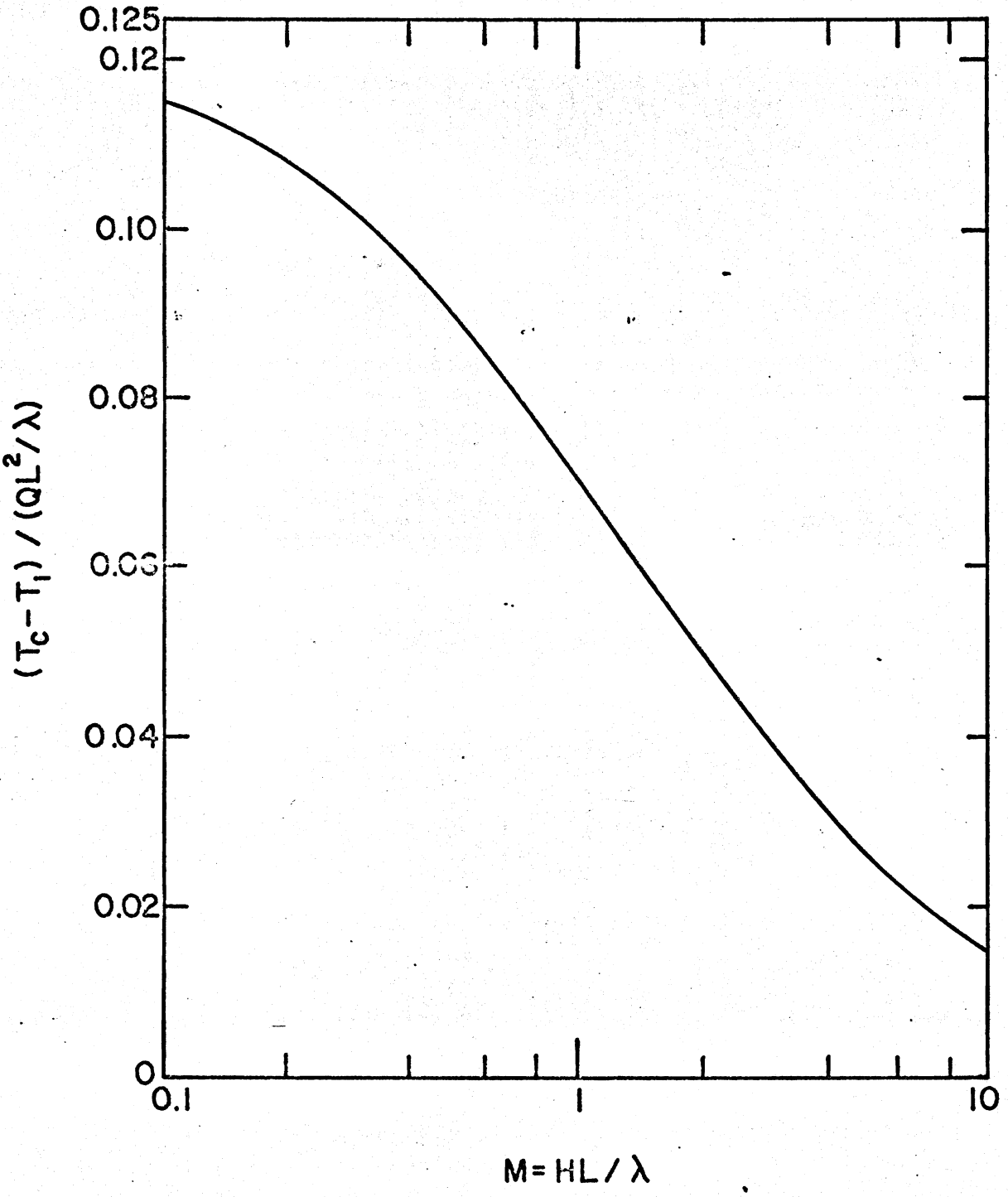

Fig. 16. Conduction-radiation results for the large path length limit.

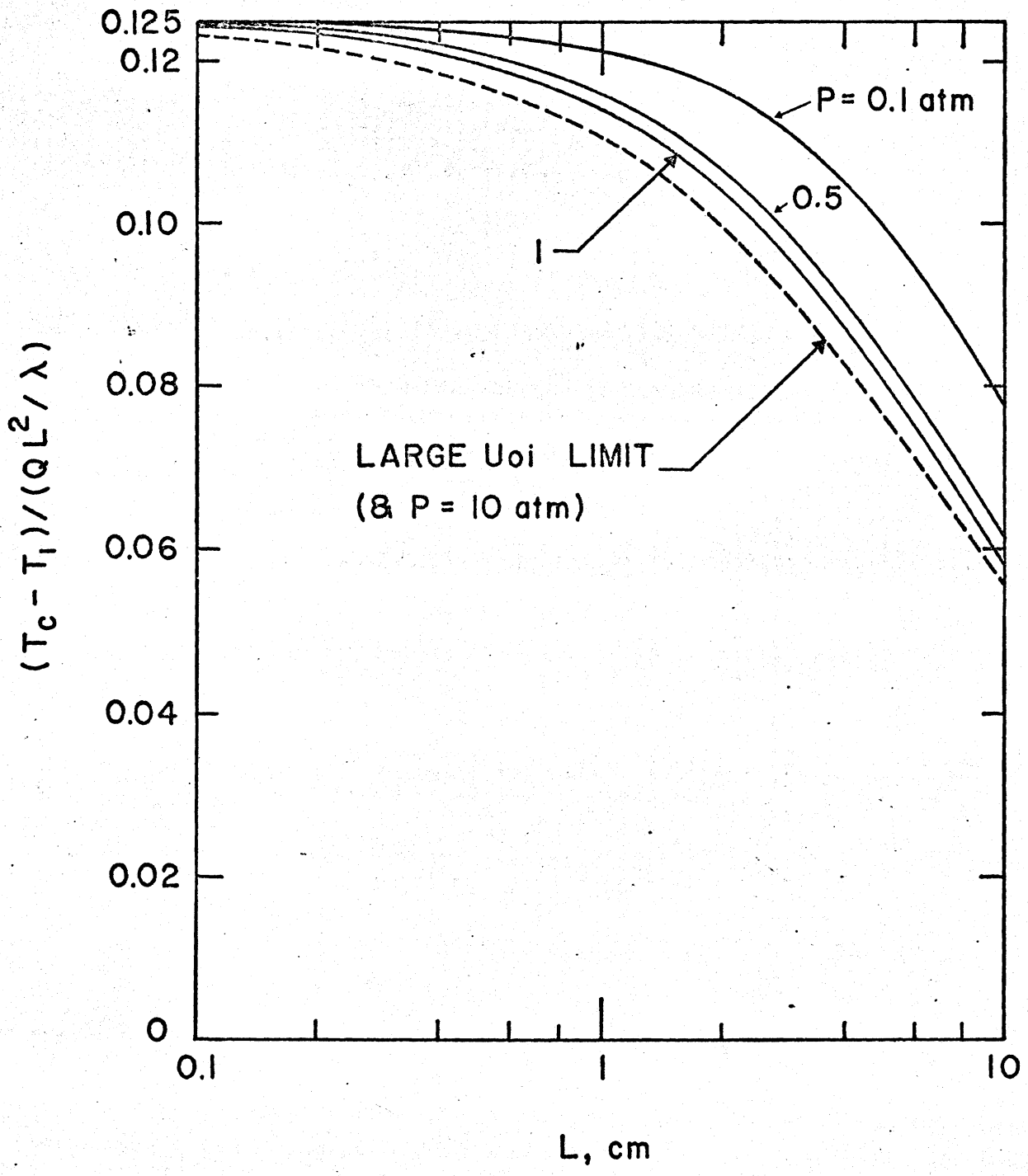

Fig. 17. Conduction-radiation results for CO_2 with T_1 = 500°K.

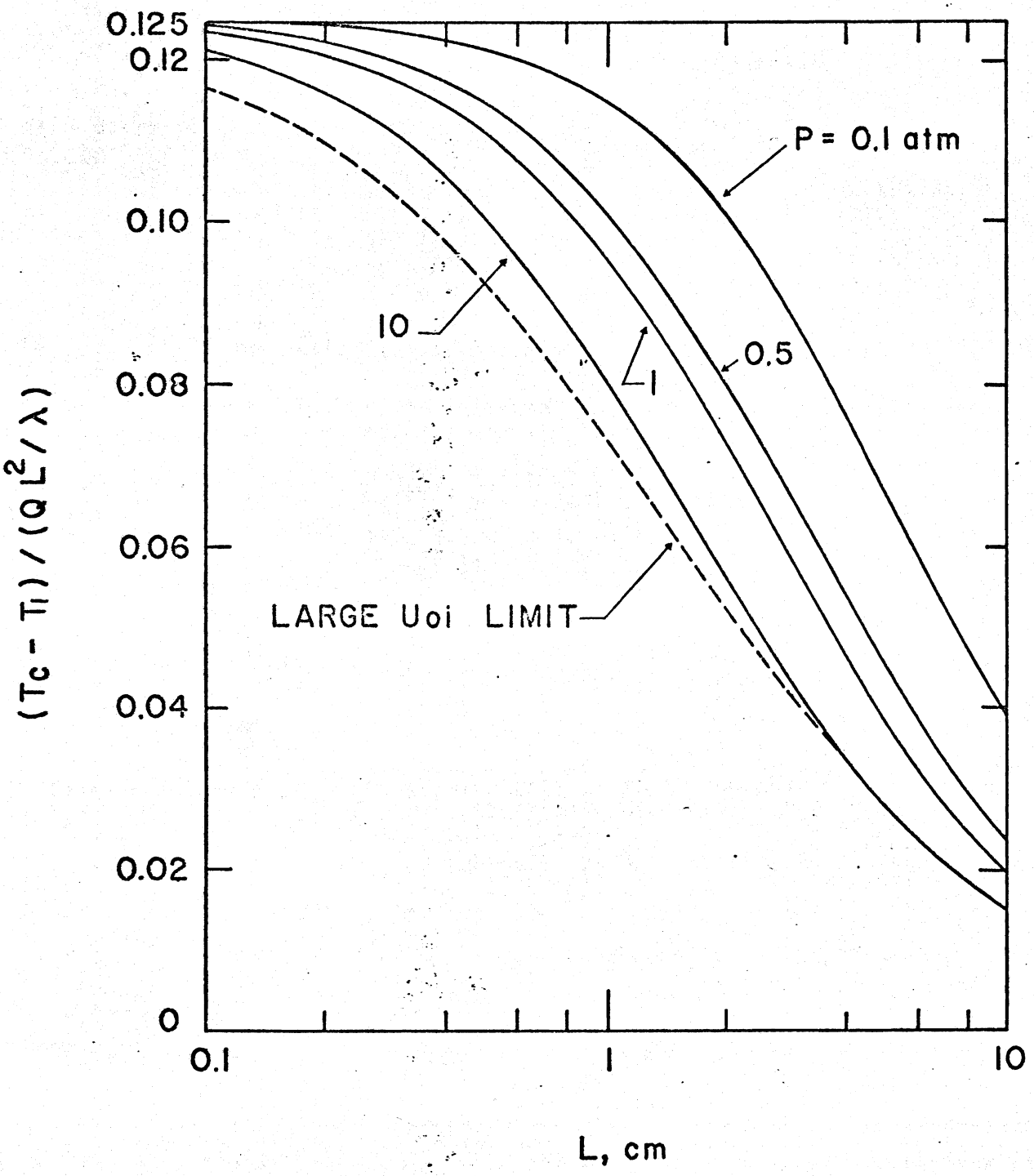

Fig. 18. Conduction-radiation results for CO_2 with T_1 = 1,000°K.

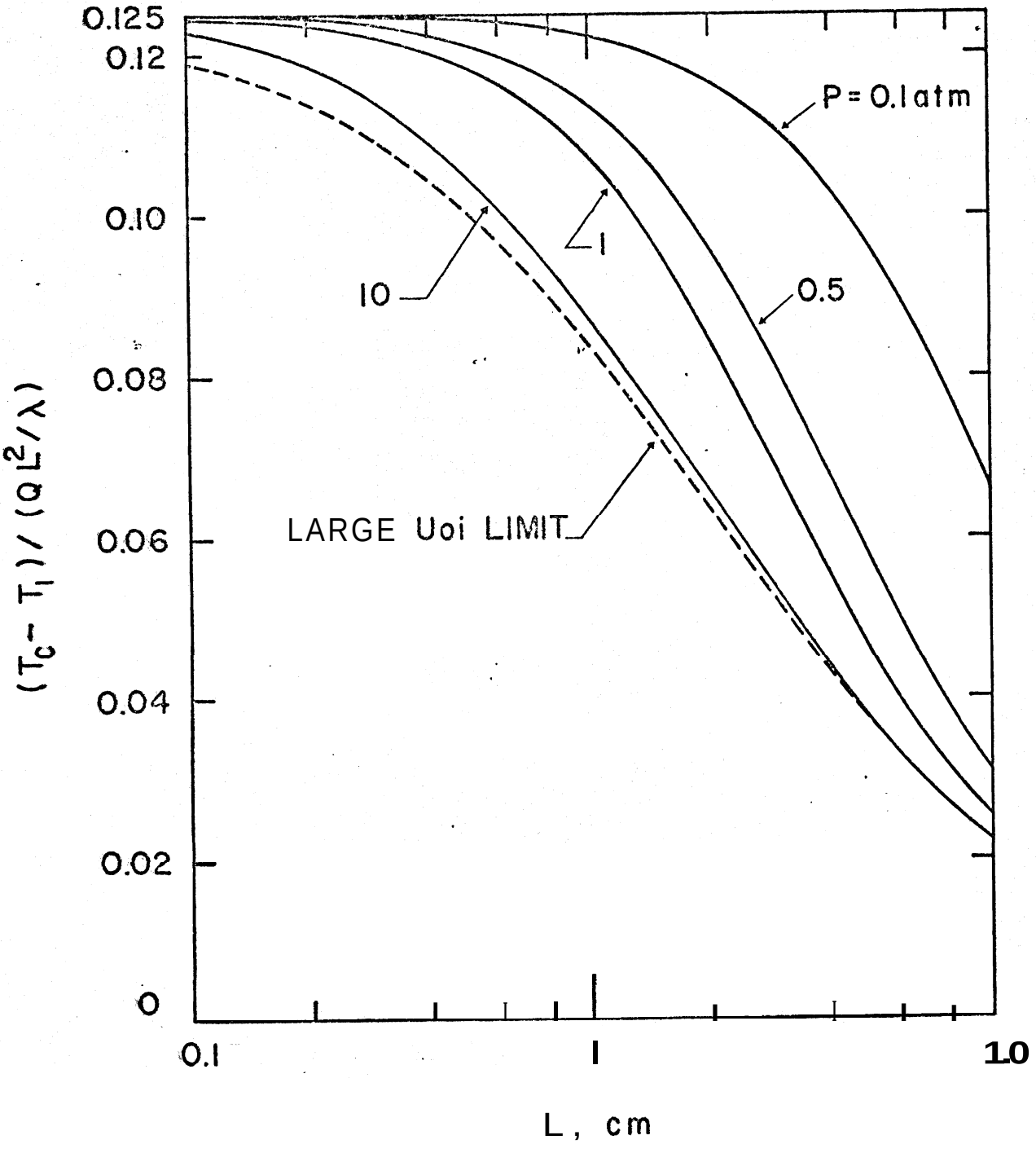

Fig. 19. Conduction-radiation **results** for H_2O with T_1 = 500°K.

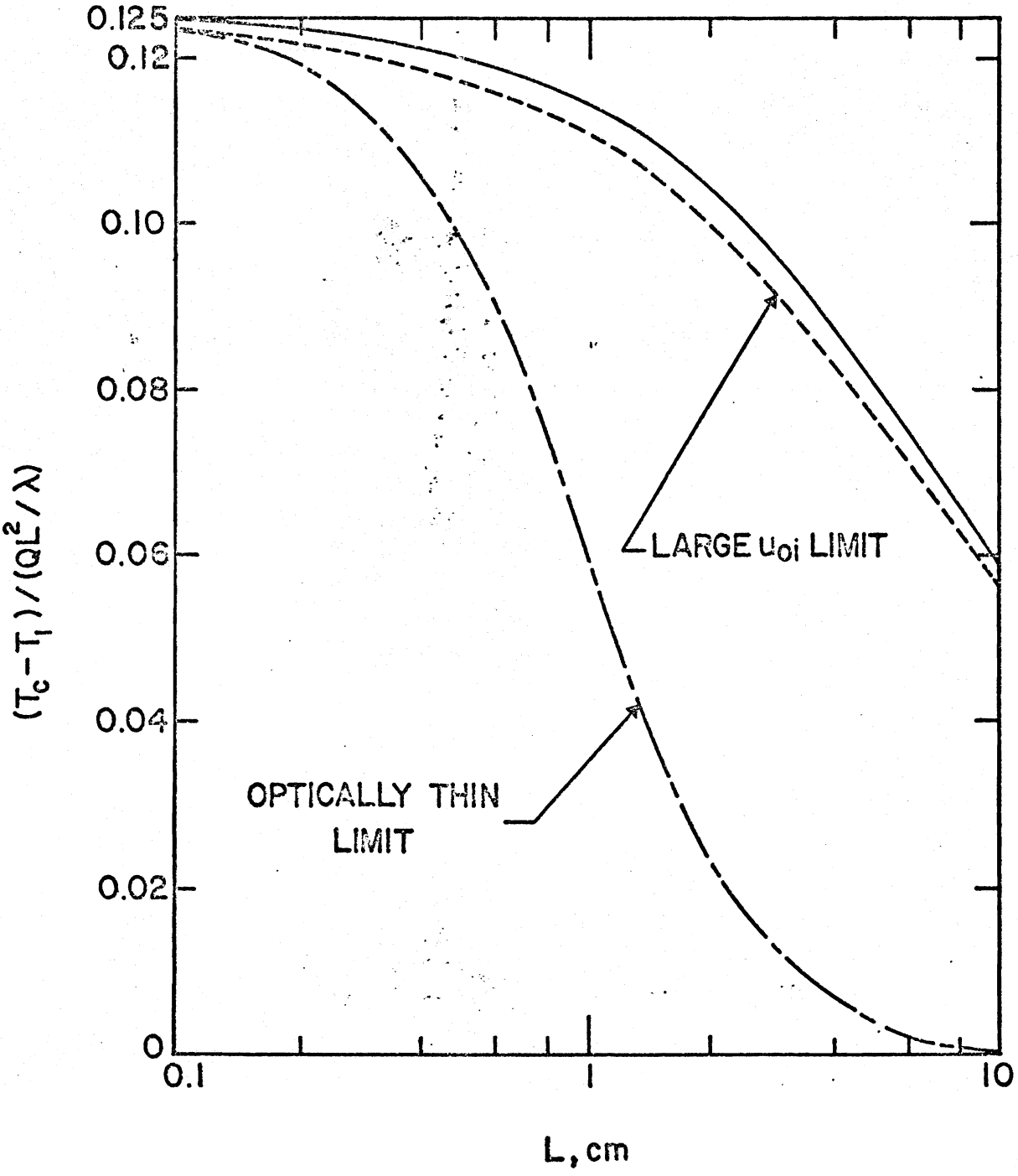

Fig. 20. Comparison of conduction-radiation solutions for CO_2 with P = 1 atm at T_1 = 500°K.

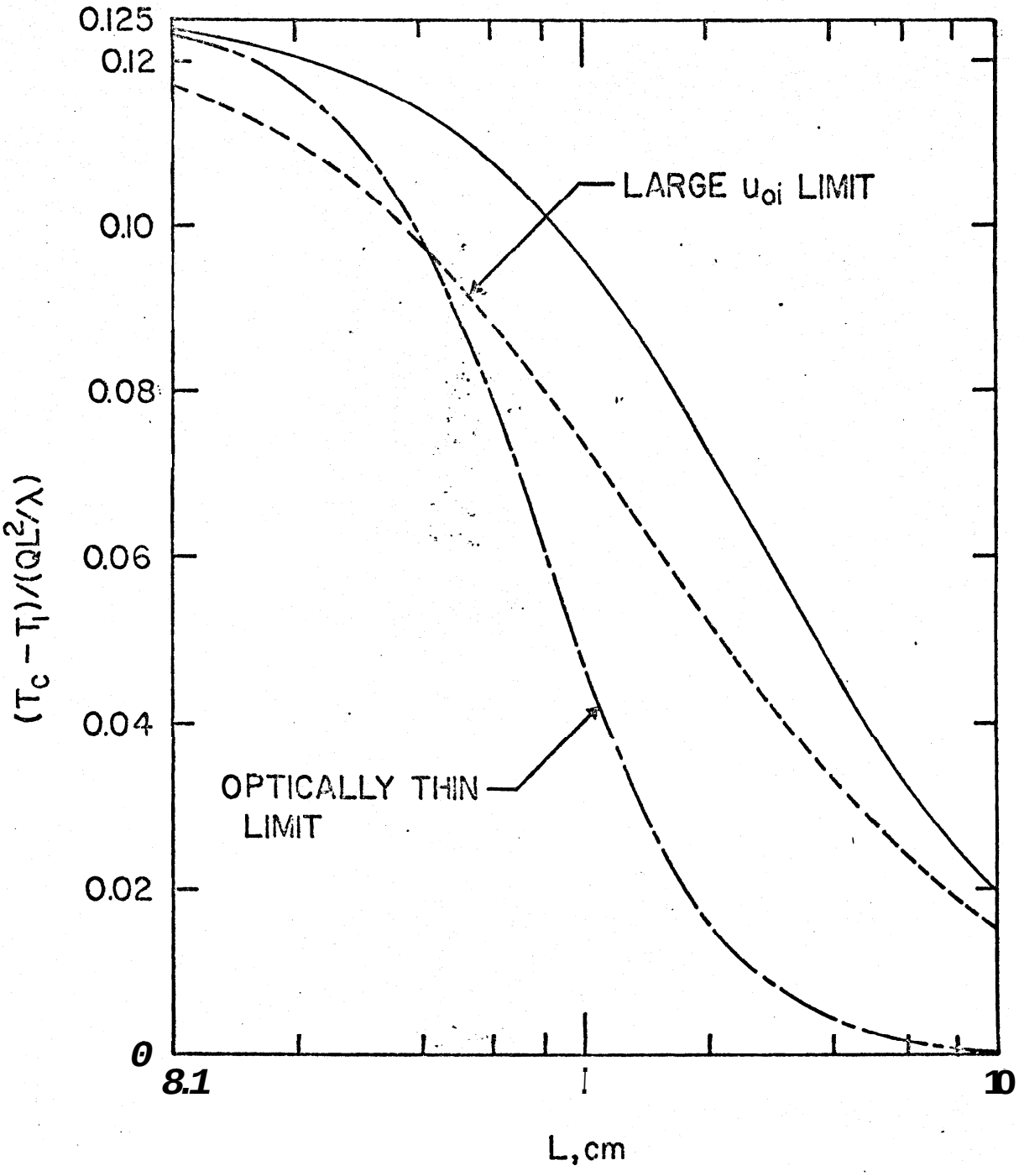

Fig. 21. Comparison of conduction-radiation solutions for CO_2 with P = .1 atm and T_1 = 500°K.

not the case at higher temperatures, for which a greater departure from the large path length limit exists. This is evident from Fig. 21, where the optically thin limit is seen to be the appropriate limiting form for small values of L.

Comparative results for CO, CO_2, H_2O, and CH_4 are shown in Figs. 22 and 23 for a pressure of one atmosphere and wall temperatures of 500°K and 1,000°K, respectively. In Fig. 22, with the exception of CO_2, the results do not correspond closely to the large path length limit, although the relative positions of the curves coincide very nearly with that indicated by the interaction parameter for large path lengths (see Fig. 15). The only exceptions are the CO and CH_4 curves showing less of a radiative interaction effect, relative to CO_2, than is indicated by Fig. 15. This is evidently a consequence of departures from the large path length limit for these two gases.

In Fig. 23 the relative order of the four curves, for small values of L, is characteristic of the interaction parameter for optically thin radiation (see Fig. 14). As the value of L is increased, the relative positions of the two curves turn into those discussed for Fig. 22.

From Figs. 17 through 19, it is evident that the large path length limit constitutes an upper bound upon the influence of radiative transfer on the temperature profile within the gas. The same conclusion applies to the optically thin limit, since self absorption is neglected. This fact that both limiting solutions constitute upper bounds on the radiative interaction can be employed to estimate whether or not, for a given gas, the interaction of radiation may be of importance.

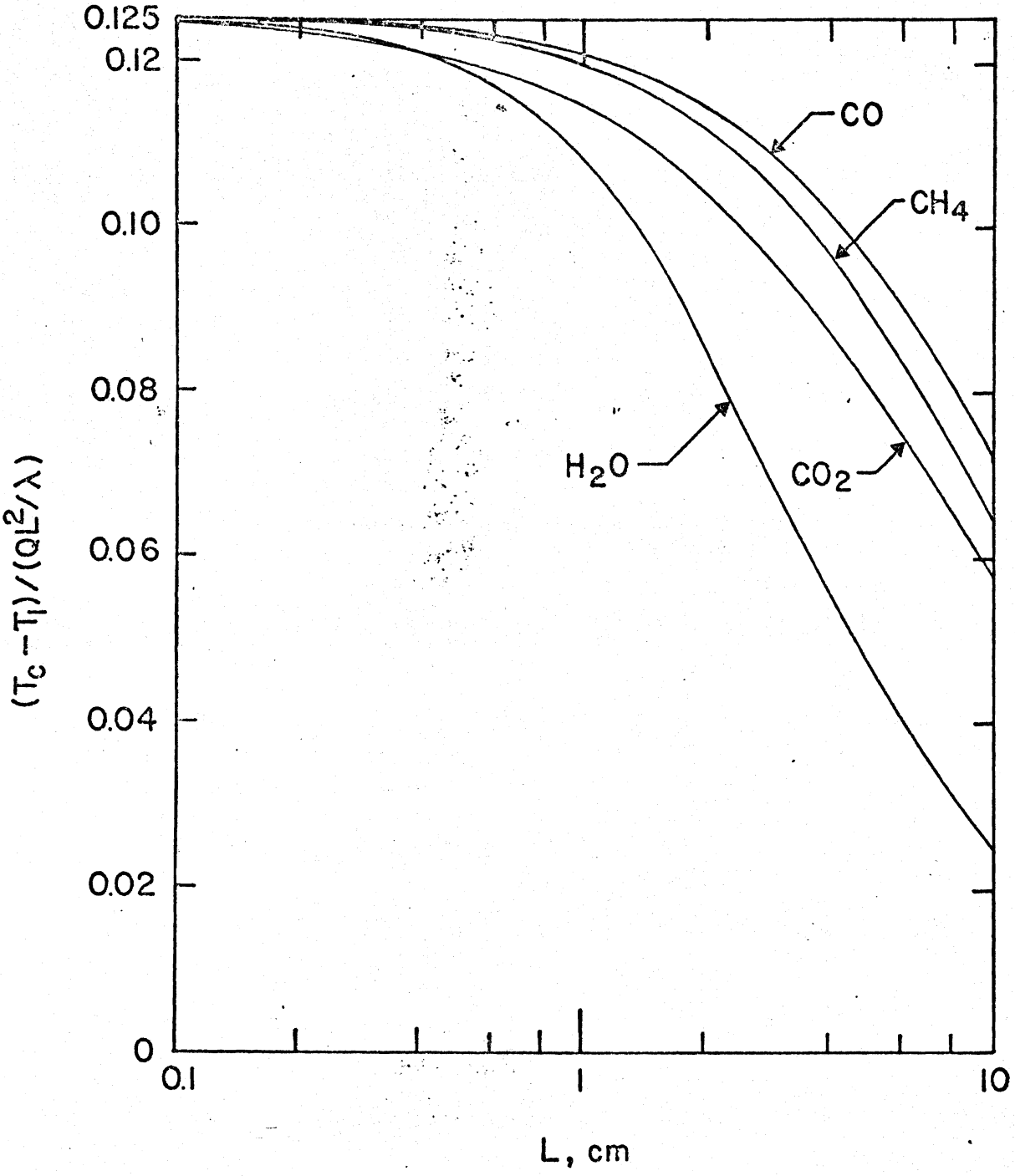

Fig. 22. Comparison of conduction-radiation results for P = 1 atm and T_1 = 500°K.

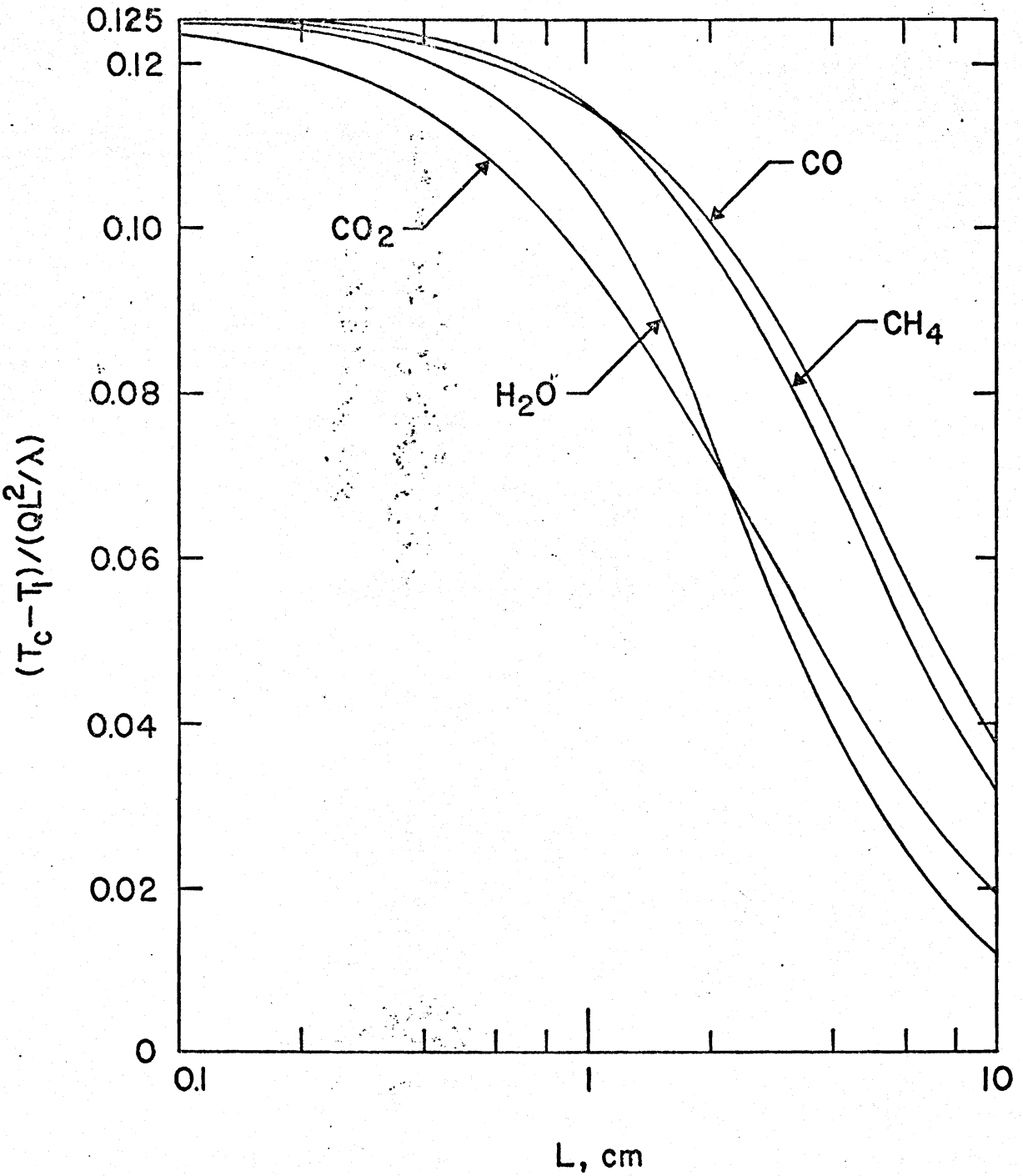

Fig. 23. Comparison of conduction-radiation results for P = 1 atm and T_1 = 1,000°K.

A final comment pertaining to radiation-conduction interaction involves the experimental measurements of Schimmel, Novotny, and Olsofka (37). The apparatus consisted of two parallel plates spaced 2.55 cm apart and maintained at different temperatures, such that there was net energy transfer from one surface to the other. Temperature profiles were obtained with a Mach-Zehnder interferometer for pure CO_2 and N_2O, and for mixtures of CO_2-CH_4 and CO_2-N_2O. The data were compared with analytical results based upon the method of solution as employed in the present section. Agreement between the experimental and analytical results was excellent. In particular, the invariance of the temperature profile upon gas pressure in the large path length limit was clearly illustrated.

C. VIBRATIONAL NONEQUILIBRIUM

In most radiative transfer analyses the assumption of local thermodynamic equilibrium is employed. There are, however, physical situations for which such an assumption is not justified. The purpose of this subsection is to investigate the possible influence of vibrational nonequilibrium upon infrared gaseous radiation. The illustrative physical models are the same as previously considered in Sections IV-A and IV-B.

Only a limited number of nonequilibrium analyses are available in the literature pertaining to infrared radiative transfer. Goody (6) utilized the nonequilibrium transfer equation, eq. (55), to derive an expression for the heating rate due to a vibration-rotation band in a plane atmosphere. The specific application involved the 15μ carbon dioxide band. The linearized form of the nonequilibrium transfer equation was employed by Gilles (27), and Gilles and Vincenti (28) to obtain an

expression for the radiative flux, with application to acoustics and flow through shock waves. Since an average absorption coefficient was used, their analysis is analogous to a modified gray gas analysis and does not account for the actual band structure. A formulation for energy transfer by radiation and conduction, in the presence of vibrational nonequilibrium, has been presented by Wang (43). It was indicated that the source function, in general, satisfies a time-dependent equation involving Planck's function, the mean intensity of radiation, and a parameter representing the relative importance of collisional and radiative relaxations. Other nonequilibrium studies pertaining to atmospheric applications are given by Thomas (44) and Oxenius (45, 46), and an application involving radiation gas dynamics is presented by Mermangen (47).

In the present investigation, the radiative flux equation, eq. (68), formulated in terms of the total band absorptance and the nonequilibrium parameter η/η_r, is employed. Results are presented for diatomic gases in general and carbon monoxide in particular. The method of analysis may, however, be extended to multiple band gases. This extension to include vibrational nonequilibrium will be illustrated for the physical systems described in Sections IV-A and IV-B.

For the case in which radiation is the only mode of energy transfer, a combination of eqs. (68), (73), and (74) yields

$$\xi - 1/2 = \frac{3u_o}{2}\int_o^{\xi}[\phi^*(\xi') - \frac{1}{4u_o}(\frac{\eta}{\eta_r})]\bar{A}'[\frac{3u_o}{2}(\xi-\xi')]d\xi' - \frac{3u_o}{2}\int_{\xi}^{1}[\phi^*(\xi') - \frac{1}{4u_o}(\frac{\eta}{\eta_r})]\bar{A}'[\frac{3u_o}{2}(\xi'-\xi)]d\xi' \qquad (93)$$

where

$$\phi^* = \frac{T-T_1}{QL/H} = \frac{T-T_1}{QL/A_o} \left(\frac{de_{\omega_o}}{dT}\right)_{T_1} \tag{94}$$

For a single band gas, the definition of ϕ^* is identical to that of ϕ given by eq. (77c). Thus, ϕ^* simply denotes a dimensionless temperature profile for non-LTE. As would be expected, eq. (93) reduces to the single band form of eq. (76) for LTE (i.e., $\eta/\eta_r = 0$), and a comparison of the two equations shows that

$$\phi^*(\xi) = \phi(\xi) + \frac{1}{4u_o} \left(\frac{\eta}{\eta_r}\right) \tag{95}$$

Employing the LTE results for ϕ as given in Fig. 7, the centerline temperature is illustrated in Fig. 24 for $\beta = \infty$. Since β is the line structure parameter and is proportional to the ratio of mean line width to mean line spacing, then $\beta = \infty$ denotes the limit of overlapping lines. Results for other values of β, corresponding to situations for which line structure is important, are qualitatively the same. Figure 24 clearly illustrates the maximum influence of non-LTE under optically thin conditions, with the subsequent diminishing of the non-LTE influence as u_o increases. Note that the non-LTE results yield higher centerline temperatures than the corresponding LTE curve. As discussed in Section III-C, this is a consequence of non-LTE reducing the capability of the gas to transmit radiative energy.

Specific results are illustrated in Fig. 25 for $T_1 = 500°K$. It is evident that non-LTE can exert a considerable influence upon the radiative transfer process for low pressures. The reason for this, of course, is that η/η_r varies inversely with pressure. Similar results are illustrated in Fig. 26 for $T_1 = 1{,}000°K$, from which it is seen that the

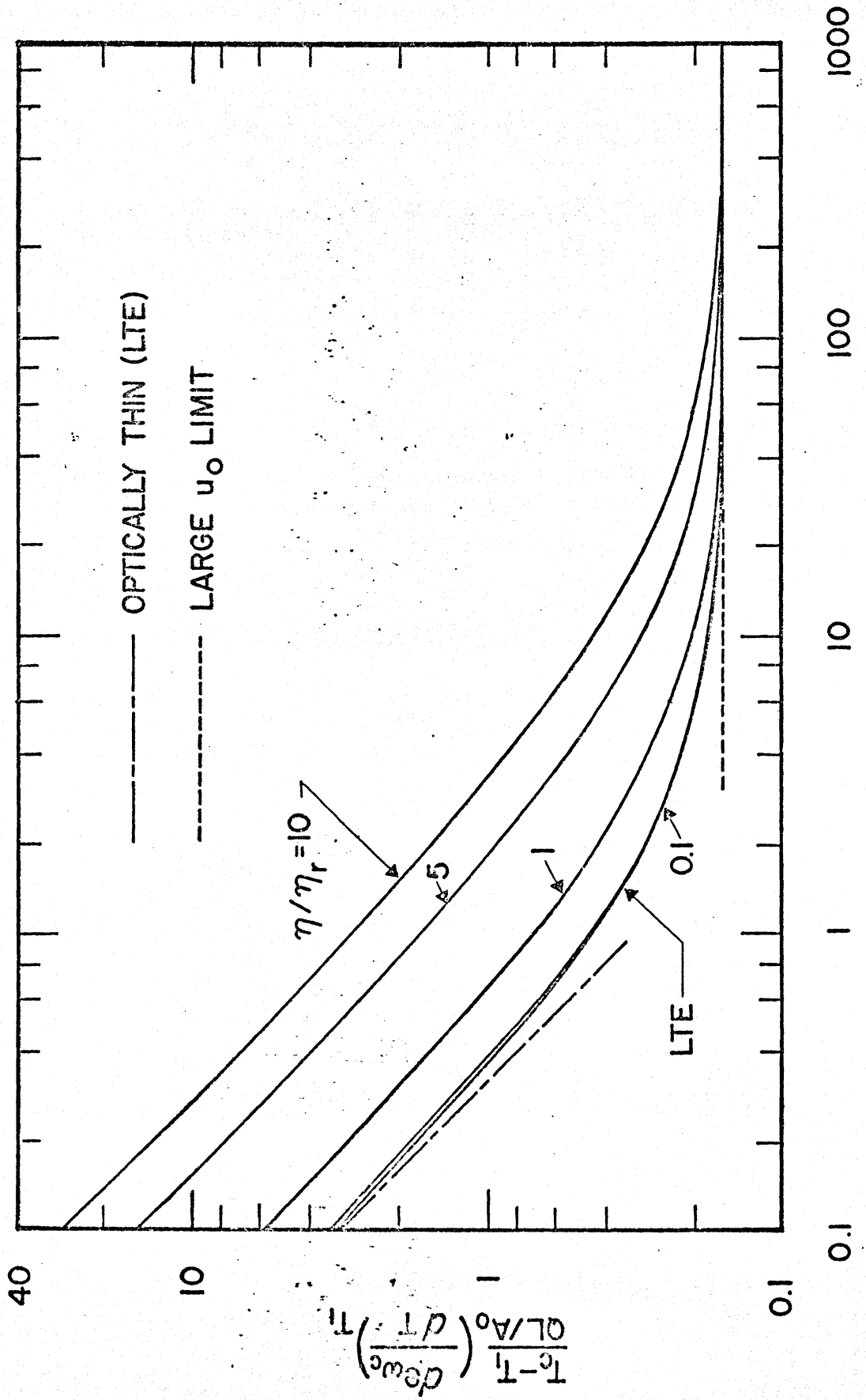

Fig. 24. Non-LTE results for a single band gas with $\beta = \infty$.

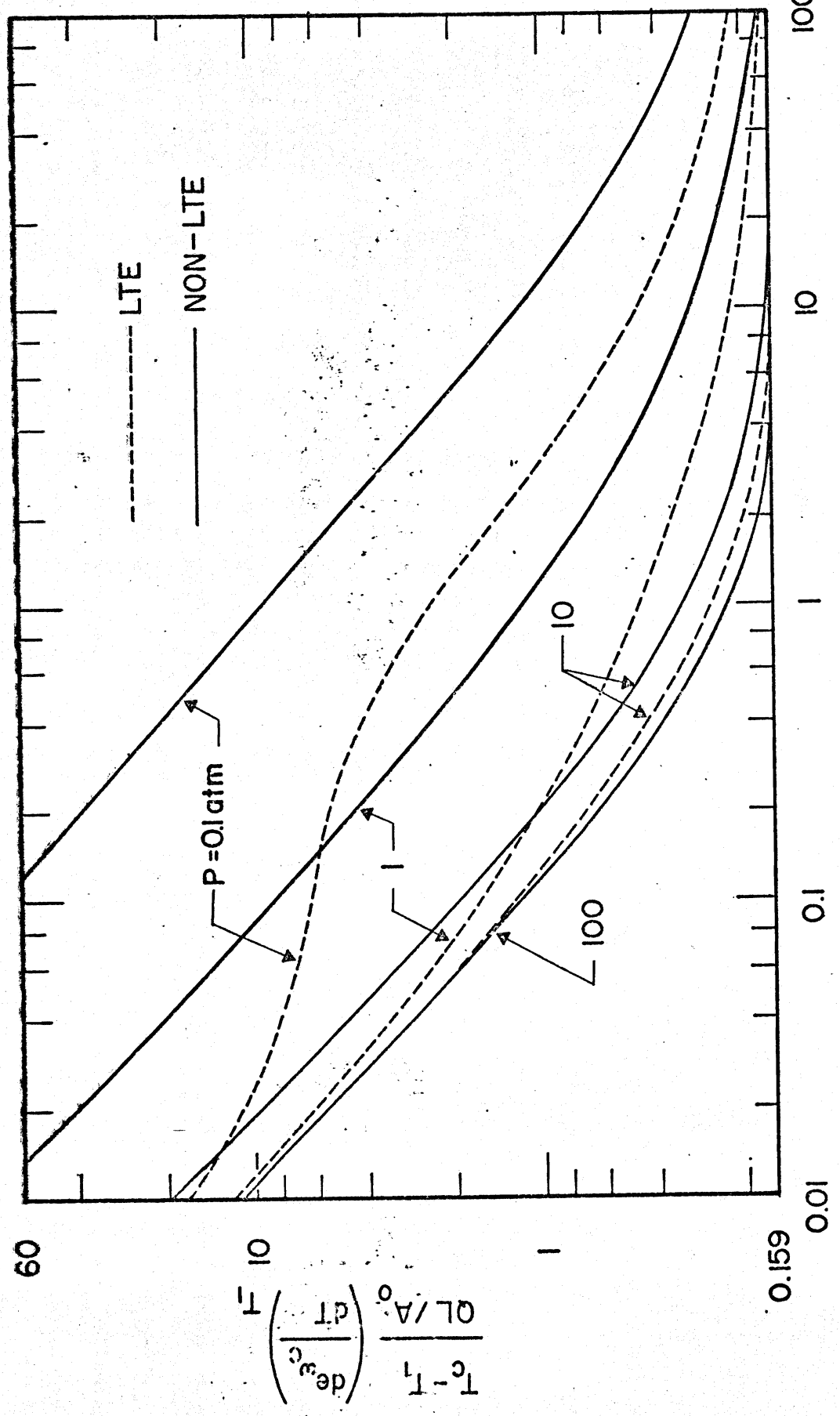

Fig. 25. LTE and non-LTE results for CO with T_1 = 500°K.

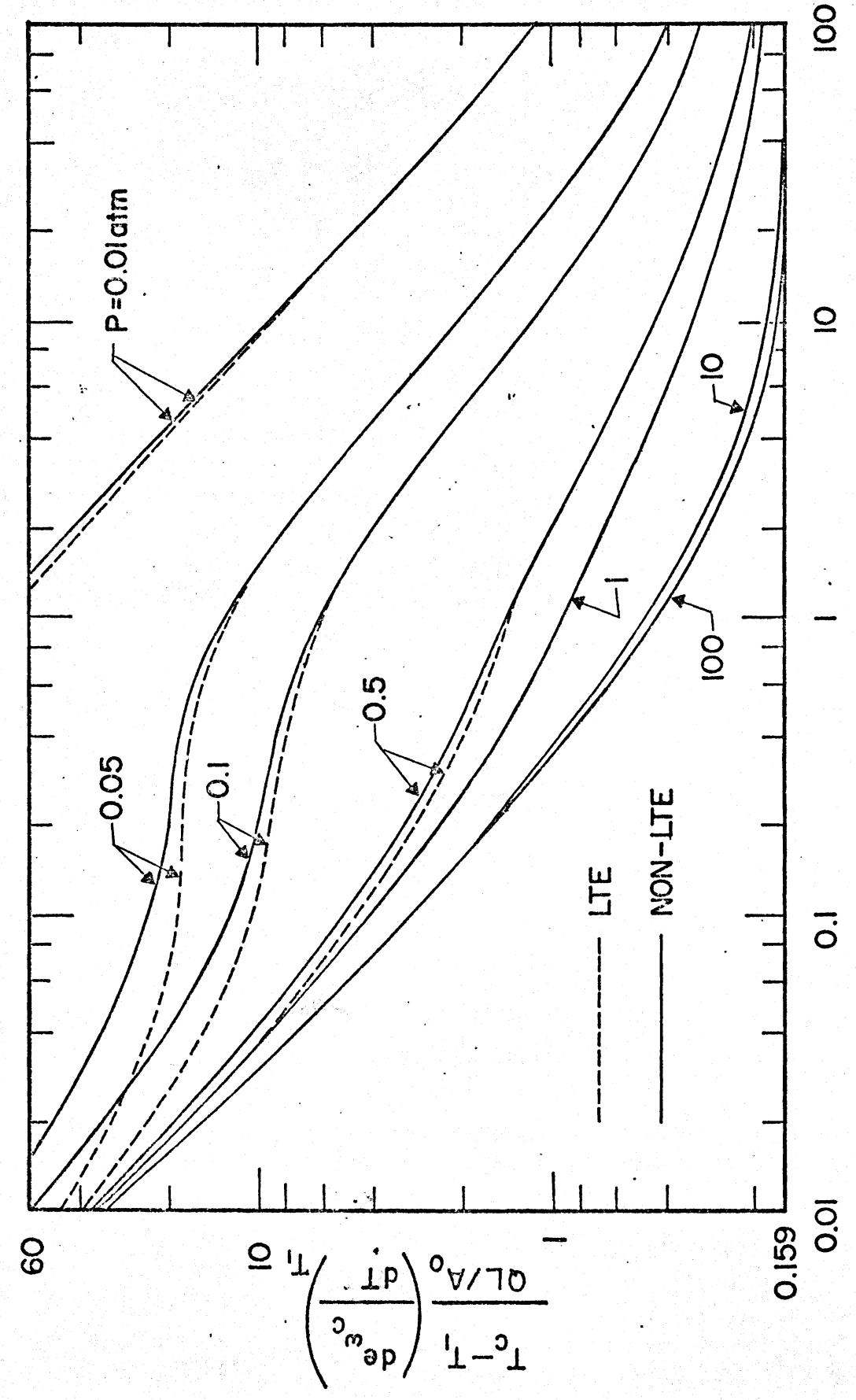

Fig. 26. LTE and non-LTE results for CO with T_l = 1000°K.

non-LTE influence is very small. This is a consequence of the strong temperature dependence of , such that the value of η/η_r at 1,000°K is approximately two orders of magnitude less than the value for 500°K.

Considering now the inclusion of molecular conduction, a combination of eqs. (68), (74), and (85) yields the appropriate energy equation as

$$\frac{d\Theta}{d\xi} + \xi - 1/2 = \frac{3Mu_o}{2}\{\int_o^{\xi}\Theta(\xi')\bar{A}'[\frac{3u_o}{2}(\xi-\xi')]d\xi' - \int_{\xi}^{1}\Theta(\xi')\bar{A}'[\frac{3u_o}{2}(\xi'-\xi)]d\xi'\} - \frac{3}{8}(\frac{\eta}{\eta_r})\{\int_o^{\xi}(1+\frac{d^2\Theta}{d\xi'^2})\bar{A}'[\frac{3u_o}{2}(\xi-\xi')]d\xi' - \int_{\xi}^{1}(1+\frac{d^2\Theta}{d\xi'^2})\bar{A}'[\frac{3u_o}{2}(\xi'-\xi)]d\xi'\} \quad (96)$$

where M is defined by eq. (92), while

$$\Theta = \frac{T-T_1}{QL^2/\lambda}$$

Equation (96) constitutes the non-LTE counterpart to the single band form of eq. (86).

Numerical solutions of eq. (96) have been obtained by the same method previously employed for LTE (48), and centerline temperatures are shown in Figs. 27 and 28 for carbon monoxide with T_1 = 500°K and 1,000°K, respectively. Recall that non-LTE effects are most pronounced for small path lengths. With reference to Fig. 27, however, this corresponds to the situation for which conduction is the predominant mode of energy transfer. Thus, for a given pressure, the non-LTE influence upon total energy transfer within the gas will vanish for either small or large values of . The former corresponds to negligible radiative transfer, while the latter denotes the large path length limit. In other words, if non-

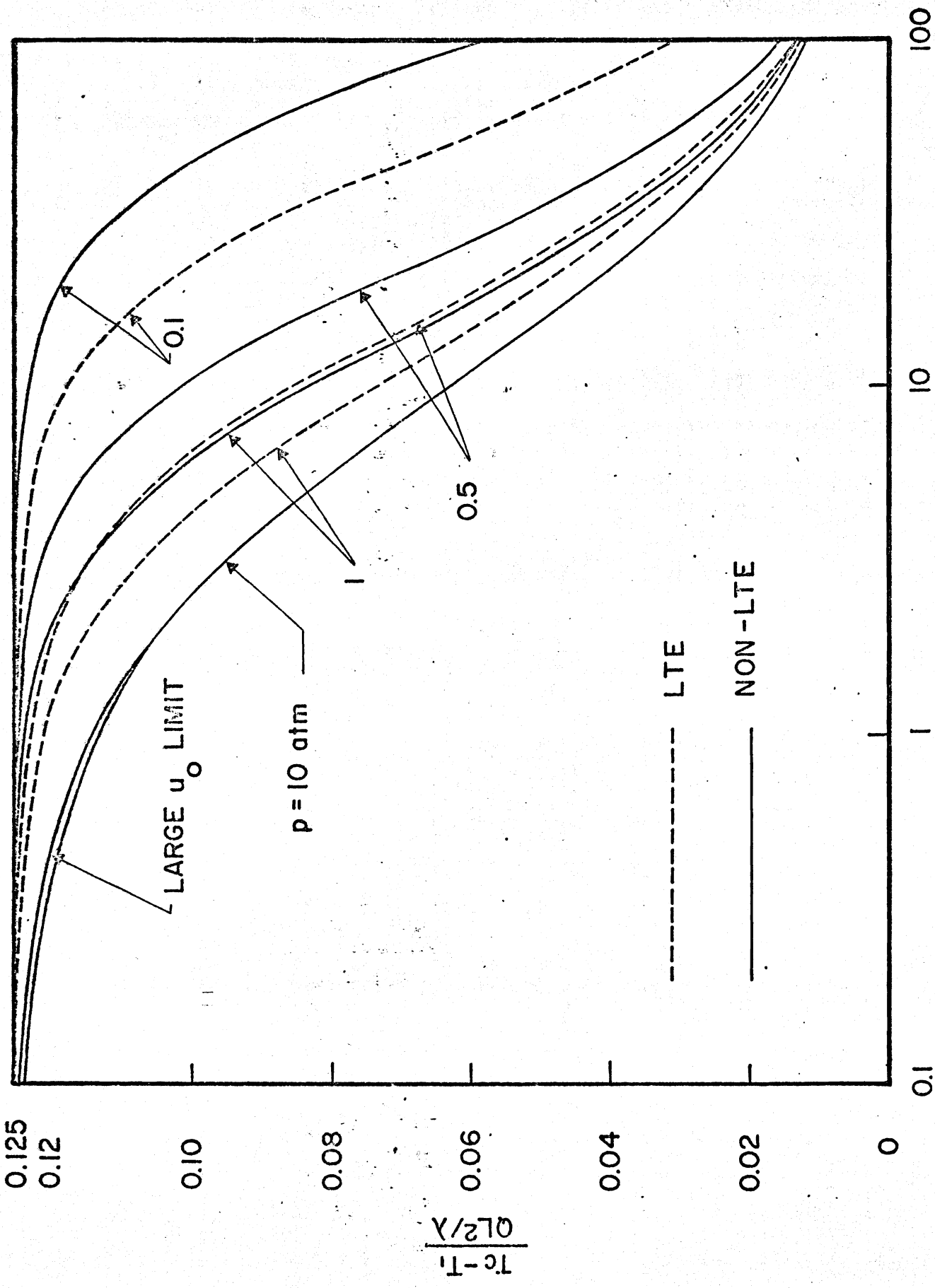

Fig. 27. Results for combined conduction and radiation with T_1 = 500°K.

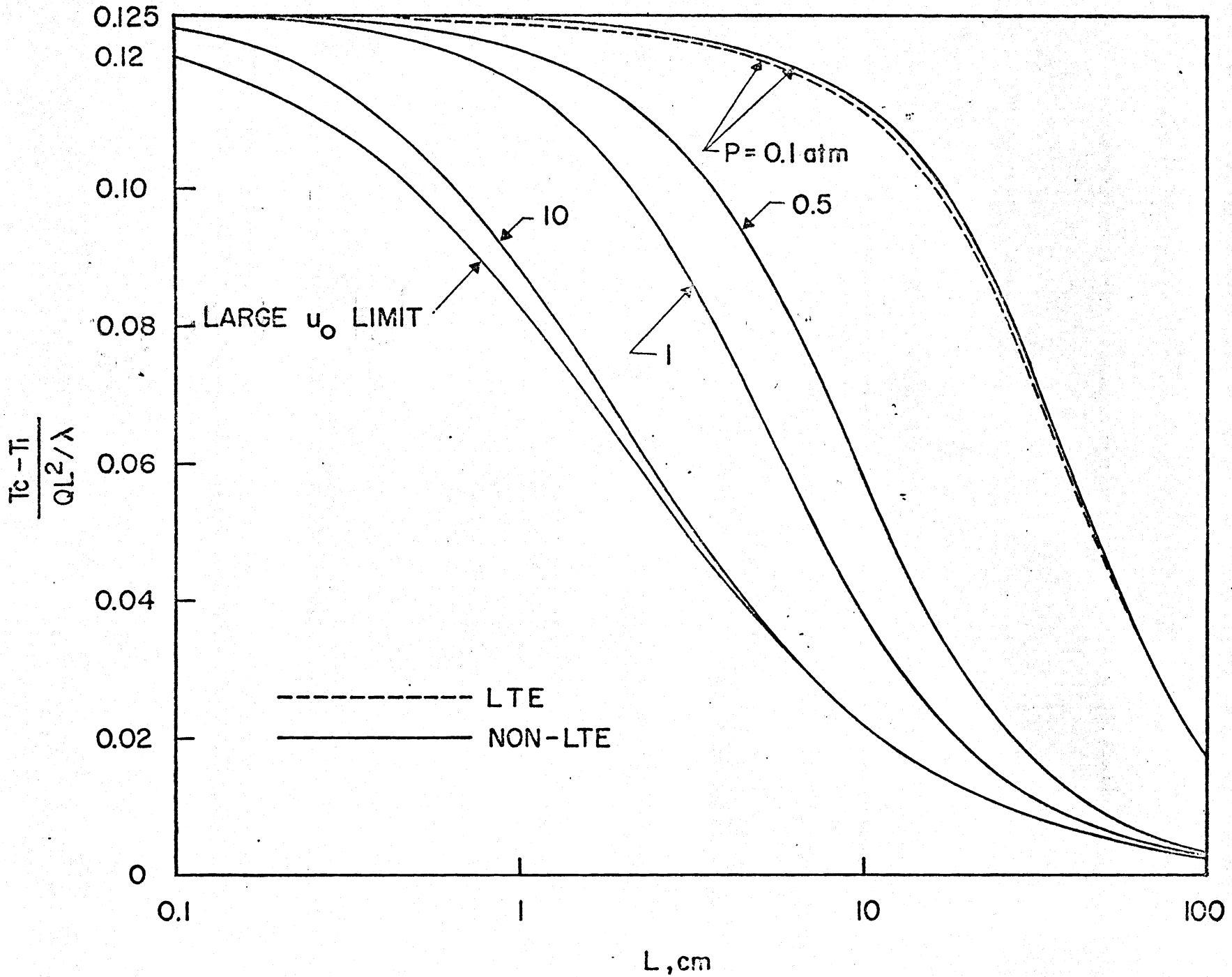

Fig. 28. Results for combined conduction and radiation with T_1 = 1000°K.

equilibrium radiation is to have a significant influence upon the energy equation, then the physical dimension of the gas system must be sufficiently large for radiation to play a dominant role, but it cannot be so large that the large path length limit is approached. In addition, of course, both pressure and temperature must be relatively low.

D. RADIATIVE EQUILIBRIUM

The preceding analyses have dealt solely with the situation for which net energy transfer is between the gas and the bounding surfaces; i.e., there is no net radiative transfer from one surface to the other. It will thus be of interest to consider briefly the opposite extreme for which the net radiative transfer is strictly between the surfaces. This is the case of radiative equilibrium, for which, with reference to Fig. 6, the surface temperatures T_1 and T_2 are not equal, and there is no other mechanism of energy addition or transfer within the gas. The energy equation is thus

$$\frac{dq_R}{dy} = 0$$

For the sake of brevity, consideration will be given only to the large path length limit, and upon summing eq. (68) over all bands, linearizing the resulting equation through the use of eq. (74), and taking the large path length limit for which $\overline{A}'(u) = 1/u$, the integral equation describing the temperature profile for radiative equilibrium follows to be (49)

$$\int_0^1 \frac{d\theta}{d\xi'} \frac{d\xi'}{\xi-\xi'} = 0 \tag{97}$$

where again $\xi = y/L$, while

$$\theta = \frac{T-T_2}{T_1-T_2}$$

As with eq. (80), the summation over individual bands vanishes in the large path length limit. The solution to eq. (97) yields (38)

$$\theta(\xi) = \frac{1}{2} + (1/\pi) \sin^{-1}(1-2\xi) \tag{98}$$

This temperature profile is illustrated in Fig. 29 together with the result for the diffusion (Rosseland) limit.

The net radiative heat flux between the plates may in turn be determined by employing eq. (98) in the expression for the radiative flux q_R, with the result that (49)

$$\frac{q_R}{4\sigma T_1^3(T_1-T_2)} = 1 - \frac{1}{4\sigma T_1^3} \sum_{i=1}^{n} A_{oi} \left(\frac{de_{\omega_i}}{dT}\right)_{T_1} \ln\left(\frac{3S_i PL}{8A_{oi}}\right) \tag{99}$$

This has been evaluated for several gases and is illustrated in Fig. 30. Since the ordinate value of unity corresponds to the transparent limit, the effectiveness of each of these gases in reducing the net radiative flux is clearly illustrated. Furthermore, for conditions under which the large path length limit does not apply, it may readily be shown that eq. (99) constitutes a lower limit on radiative transfer.

It is interesting to note the difference between the present results and those of Section III-A, which dealt with a uniform heat source within a gas bounded by symmetrically heated plates. Again these constitute two opposite extremes in that the net radiative transfer is solely between surfaces in the present situation, whereas it is between the gas and the bounding surfaces in the former case, and recall from

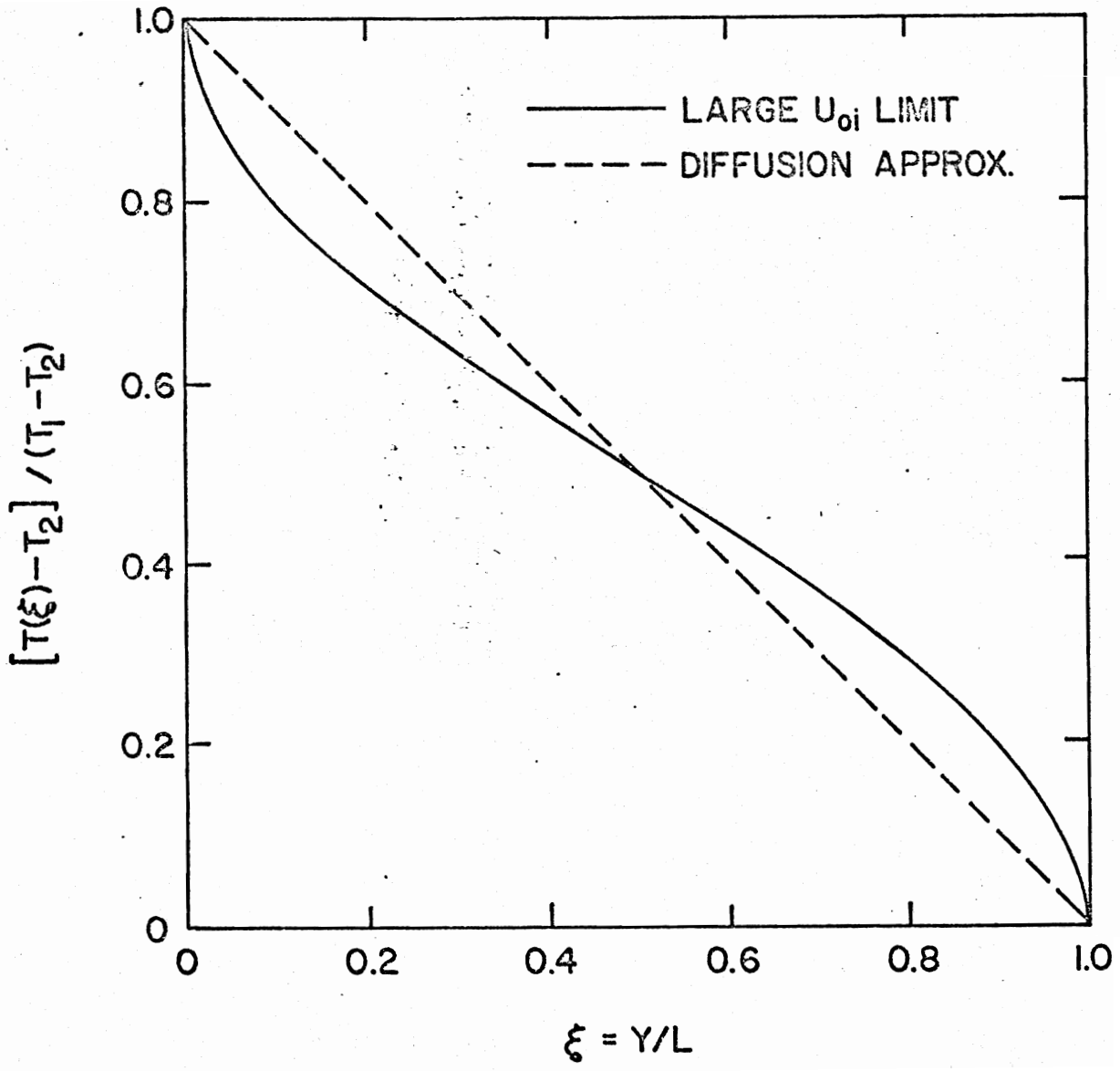

Fig. 29. Temperature distribution for radiative equilibrium in the large path length limit.

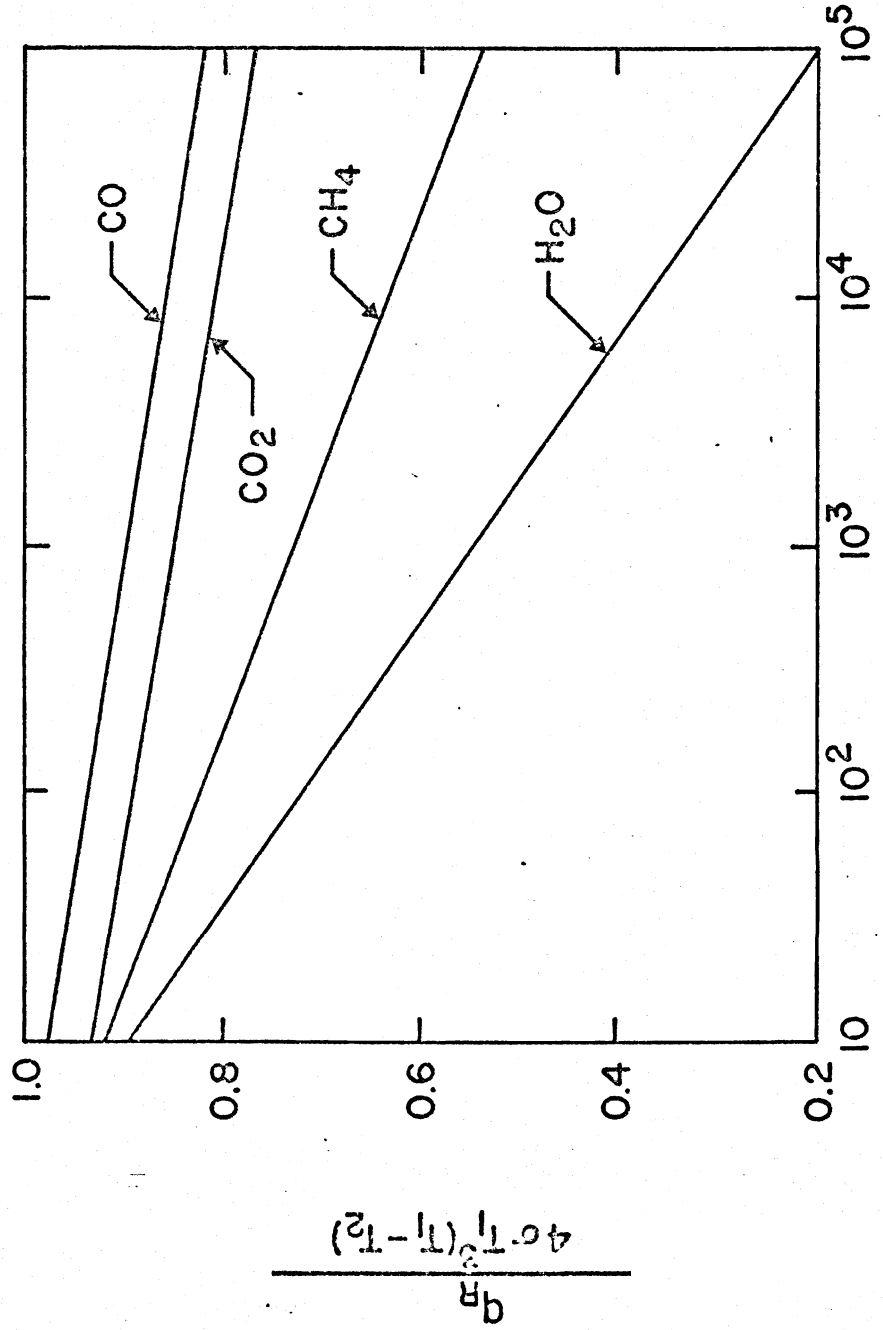

Fig. 30. Radiative flux results for radiative equilibrium and T_1 = 500°K.

Section 111-A that the band intensities S_i do not appear in the large path length limit. This absence can be traced to the fact that the central portion of a band, since it is saturated in the large path length limit, has no effect upon the net radiative transfer between the gas and the bounding surfaces. In other words, net radiative transfer takes place only in the wing regions of the bands, and the extent of the wings depends only on A_{oi}. This is not the case in the present situation, however, since the reduction in the net radiative transfer between surfaces will depend upon the extend of the saturated central portion of the bands, and hence eq. (99) contains both of the band parameters A_{oi} and S_i.

V. CONCLUDING REMARKS

The intent of the present chapter has been to investigate the basic features of infrared gaseous radiation through use of extremely simple and illustrative physical models, and no attempt has been made to describe specific applications. There does exist, however, a body of literature pertaining to the inclusion of spectroscopic information into radiative transfer analyses involving the structure and dynamics of planetary atmospheres. In such investigations infrared gaseous radiation constitutes an important mechanism of energy transfer, and for the most part, as in the present chapter, the kernel function for the radiative flux is formulated in terms of the band absorptance (or transmission function). Normally, however, attention is directed towards numerical solutions for specific planetary conditions, and little emphasis is placed upon the basic features of the radiative transfer process.

A partial summary of atmospheric radiation analyses includes the investigations of Manabe and coworkers (50, 51, 52, 53) for Earth; studies of the structure of the Martian atmosphere by Prabhakara and Hogan (54), Ohring and Mariano (55, 56), and Gierasch and Goody (57, 58); and the analysis of the atmosphere of Venus above the cloud tops by Bartko and Hanel (59). A wealth of information may further be found in the book by Goody (6).

ACKNOWLEDGMENTS

The authors wish to express their gratitude to their colleagues, Professors P. Varanasi and L.S. Wang, for numerous discussions and advice. Much of the work reported herein was supported by the National Science Foundation.

NOMENCLATURE

A	total band absorptance, cm^{-1}
A_j	total absorptance of a single line
A_o	band width parameter (correlation quantity), cm^{-1}
$\bar{A}(u,\beta)$	dimensionless band absorptance, $\bar{A} = A/A_o$
B	rotational constant, cm^{-1}
B_ω	black-body intensity at local temperature
$B_{1\omega}$, $B_{2\omega}$	spectral surface radiosities, $(watts\text{-}cm^{-2})/cm^{-1}$
c	speed of light
e_ω	Planck's function, $(watts\text{-}cm^{-2})/cm^{-1}$
e_{ω_o}, e_{ω_c}	Planck's function evaluated at band center
$e_{1\omega_o}$, $e_{1\omega_c}$	Planck's function evaluated at temperature T_1
E_v	vibrational energy
E_v^*	equilibrium vibrational energy
h	Planck's constant
H	gas property for the large path length limit, eq. (82)
I_ω	specific intensity
J_ω, J_{ω_o}	source function
k	Boltzmann constant
K	gas property for the optically thin limit, eq. (79)
L	distance between plates, *cm*
M	radiation-conduction interaction parameter, eq. (92)
N	radiation-conduction interaction parameter, eq. (89)
P	gas pressure, atm
P_e	equivalent (effective) broadening pressure
q_R	total radiative heat flux, $watts/cm^2$

$q_{R\omega}$	spectral radiative flux, $(\text{watts-cm}^{-2})/\text{cm}^{-1}$
Q	heat source or sink, watts/cm^3
s	distance along direction of radiative propagation
S,S(T)	total band intensity, $\text{atm}^{-1}\text{-cm}^{-2}$
S_j	line intensity
T	temperature, kinetic temperature, °K
T_o	reference temperature (equilibrium)
T_1, T_2	surface temperature
u	dimensionless coordinate, $u = SPy/A_o$
u_o	dimensionless path length, $u_o = SPL/A_o$
y	physical coordinate
α_ω	spectral band coefficient
β	line struction parameter
γ	rotationally averaged line half width, eq. (35)
$\bar{\gamma}$	vibrationally averaged line half width, eq. (39)
γ_j	line half width, cm^{-1}
ε	surface emittance
η	vibrational relaxation time, sec
η_r	radiative life time of vibrational state, sec
θ	dimensionless temperature, eq. (86)
Θ	dimensionless temperature, eq. (97)
K_ω	equilibrium spectral absorption coefficient, cm^{-1}
κ_P	Planck mean coefficient, cm^{-1}
$\bar{\kappa}$	mean absorption coefficient, $\bar{\kappa} = SP/\Delta\omega$
λ	thermal conductivity, $(\text{watts-cm}^{-2})/°K$
v	frequency
ρ	density

σ	Stefan-Boltzmann constant
ϕ	dimensionless function, eq. (77c)
ϕ^*	dimensionless function, eq. (94)
Ω	solid angle
ω	wave number, cm^{-1}
ω_o, ω_c	wave number at the band center, cm^{-1}

REFERENCES

1. C.L. Tien, Advan. Heat Transfer 5, 253 (1968).
2. L.M. Trafton, Astrophys. J. 147, 765 (1967).
3. J.S. Hogan, S.I. Rasool, and T. Encrenaz, J. Atmos. Sci. 26, 898 (1969).
4. G. Yamamoto, M. Tanaka, and T. Aoki, JQSRT 9, 371 (1969).
5. S.S. Penner, Quantitative Molecular Spectroscopy and Gas Emissivities, Addison-Wesley, Reading, Mass., 1959.
6. R.M. Goody, Atmospheric Radiation, Oxford University Press, London, 1964.
7. D.K. Edwards and W.A. Menard, Appl. Optics 3, 621 (1964).
8. D.K. Edwards and W.A. Menard, Appl. Optics 3, 874 (1964).
9. D.K. Edwards, Appl. Optics 4, 1352 (1965).
10. D.K. Edwards, L.K. Glassen, W.C. Hauser, and J.S. Tuchscher, J. Heat Transfer 86, 219 (1967).
11. C.L. Tien and J.E. Lowder, Int. J. Heat Mass Transfer 9, 698 (1966).
12. R. Goody and M.J.S. Belton, Planet. Space Sci. 15, 247 (1967).
13. Ya. B. Zel'dovich and Yu. P. Raizer, Physics of Shock Waves and High-Temperature Hydrodynamic Phenomena, Vols. I and II, Academic Press, N.Y., 1967.
14. J. Gille and R. Goody, J. Fluid Mechs. 22, 47 (1964).
15. L.S. Wang, JQSRT 8, 851 (1968).
16. L.S. Wang, JQSRT 8, 1233 (1968).
17. W.G. Vincenti and C.H. Kruger, Jr., Introduction to physical Gas Dynamics, John Wiley and Sons, New York, 1965.
18. N.W. Bazley and E.W. Montroll, J. Chem. Phys. 28, 700 (1958).
19. L.L. Northup and C.T. Hsu, Phys. of Fluids 11, 1375 (1968).
20. J.P. Hodgson and R.J. Hine, J. Fluid Mechs. 35, 171 (1969).
21. W.J. Hooker and R.C. Millikan, J. Chem. Phys. 38, 214 (1963).
22. R.C. Millikan and D.R. White, J. Chem. Phys. 39, 3209 (1963)
23. C.J.C.M. Simpson, K.D. Bridgeman, and T.R.D. Chandler,

J. Chem. Phys. 49, 5GY (1968).

24. R.C. Millikan, Phys. Rev. Letters 8, 253 (1962).

25. M.G. Ferguson and R.W. Read, Trans. Faraday Soc. 61, 1559 (1965).

26. R.C. Millikan, Molecular Relaxation Processes, Academic Press and Chemical Society of London, 1966.

27. S.E. Gilles, "Flow with Coupled Radiative and Vibrational Non-equilibrium in a Diatomic Gas", Ph.D. Dissertation, Stanford University (1968).

28. S.E. Gilles and W.G. Vincenti, JQSRT 10, 71 (1970).

29. S.N. Tiwari, "Infrared Radiative Energy Transfer in Nongray Gases", Ph.D. Dissertation, State University of New York at Stony Brook (1969).

30. E.M. Sparrow and R.D. Cess, Radiation Heat Transfer, Brooks/Cole, Belmont, Calif. (1966).

31. D.H. Sampson, Radiative Contributions to Energy and Momentum Transfer, Interscience, New York (1965).

32. R.D. Cess and S.N. Tiwari, Appl. Sci. Res. 20, 25 (1969).

33. R.D. Cess, P. Mighdoll, and S.N. Tiwari, Int. J. Heat Mass Transfer 10, 1521 (1967).

34. R. Grief and I.S. Habib, J. Heat Transfer 91, 282 (1969).

35. R.D. Cess and S.N. Tiwari, Appl. Sci. Res. 19, 439 (1968).

36. A.C. Cogley, W.G. Vincenti, and S.E. Gilles, AIAA J. 6, 551 (1968).

37. W.P. Schimmel, J.L. Novotny, and F.A. Olsofka, Proceedings of the Fourth International Heat Transfer Conference, Paris-Versailles, Vol. III (1970).

38. S.G. Mikhlin, Integral Equations, p. 126, Pergamon Press, Oxford (1967).

39. S.N. Tiwari and R.D. Cess, Int. J. Heat Mass Transfer 11, 1731 (1968).

40. M.A. Heaselet and R.F. Warming, Int. J. Heat Mass Transfer 8, 979 (1965).

41. D.A. Mandell, JQSRT 10, 459 (1970).

42. N.V. Tsederberg, Thermal Conductivity of Gases and Liquids, M.I.T. Press, Cambridge, Mass. (1965).

43. L.S. Wang, "The Cooling of a Gas not in Local Thermodynamic Equilibrium by Conduction and Radiation", AIAA Paper No. 69-638 (1969).

44. R.N. Thomas, Some Aspects of Non-Equilibrium Thermodynamics in the

Presence of a Radiation Field, University of Colorado Press (1965).

45. J. Oxenius, JQSRT 5, 771 (1965).

46. J. Oxenius, JQSRT 6, 65 (1966).

47. W.H. Mermagen, Phys. of Fluids 10, 1801 (1967).

48. S.N. Tiwari and R.D. Cess, JQSRT 11, 237 (1971).

49. P. Mighdoll and R.D. Cess, AIAA J. 6, 1778 (1968).

50. S. Manabe and F. Möller, Mon. Wea. Rev. 89, 503 (1961).

51. S. Manabe and R.F. Strickler, J. Atmos. Sci. 21, 361 (1964).

52. S. Manabe and R.T. Wetherald, J. Atmos. Sci. 24, 241 (1967).

53. S. Manabe and B.G. Hunt, Mon. Wea. Rev. 96, 477 (1968).

54. C. Prabhakara and J.S. Hqgan, Jr., J. Atmos. Sci. 22, 97 (1965).

55. G. Ohring and J. Mariano, J. Atmos. Sci. 23, 251 (1966).

56. G. Ohring and J. Mariano, J. Atmos. Sci. 25, 673 (1968).

57. P. Gierasch and R. Goody, Planet. Space Sci. 15, 1465 (1967).

58. P. Gierasch and R. Goody, Planet. Space Sci. 16, 615 (1968).

59. F. Bartko and R.A. Hanel, Astrophys. J. 151, 365 (1968).